Ore Geology Reviews 180 (2025) 106584

Contents lists available at ScienceDirect

Ore Geology Reviews

journal homepage: www.elsevier.com/locate/oregeorev

Recurrent granite-related mineralization along former Tethys sutures in southwestern China☆

Fucheng Yang [a,b], Rolf L. Romer [c], Xiaojun Jiang [a], Wenchang Li [a,b,d,*]

[a] Kunming University of Science and Technology, Kunming 650093, China
[b] China University of Geosciences, Beijing 100083, China
[c] Helmholtz Centre Potsdam, GFZ German Research Centre for Geosciences, Telegrafenberg D-14473 Potsdam, Germany
[d] Chengdu Center of China Geological Survey, Chengdu 610081, China

ARTICLE INFO

Keywords:
Granite-related mineralization
Multistage mineralization
Tectonic reactivation
Paleo-Tethys suture
Sanjiang Tethyan domain

ABSTRACT

The sutures of the Paleo-Tethys, Meso-Tethys, and Neo-Tethys oceans in southwestern China host many major porphyry- and/or granite-related mineral deposits. We compile age and geochemical data from these deposits. The age data show that most of these deposits are not related to the formation of the sutures, but to their later tectonic reactivation. For instance, intrusion-related deposits along fault zones in the Sanjiang area, which represent the suture of the former Paleo-Tethys Ocean, fall in one of the four age groups: 239–206 Ma, 182–162 Ma, 126–70 Ma, and 53–32 Ma. The oldest group of major porphyry- and/or granite-related deposits in the Sanjiang zone is related to the subduction and closure of the Paleo-Tethys Ocean, whereas younger deposits formed during the reactivation of Paleo-Tethys sutures during the closure of the Meso-Tethys and the Neo-Tethys oceans and during the India–Asia collision. Different types of coeval porphyry- and/or granite-related deposits occur along different segments of the same crustal-scale structure and are related to different types of intrusions: Cu (—Mo), Cu—Au, Au, and Mo (—Cu) porphyry or skarn deposits are associated with relatively oxidized rocks that were derived from the melting of subduction-modified mantle with variable contributions from the crust and W—Mo and Sn—W deposits are related to highly evolved, reduced porphyries and/or granites that originated from partial melting of metasedimentary rocks. Although the inventory of sedimentary source rocks along the sutures is controlled by the geological development before the suture formed, the later reactivation of the suture determines which source rocks become available for melting and, thus, which type of mineralization may form along different reactivated segments.

1. Introduction

The occurrence of magmatic and hydrothermal mineral deposits in belts and provinces, as well as their spatial separation in provinces of different metal association, had been recognized long before Mitchell and Garson (1981) documented the connection between tectonic setting and mineral deposits in a plate tectonic context. Whereas early tectonic interpretations of porphyry deposits of the metals Cu, Mo, Au, W, and Sn focused on the role of the subducting slab and the distance from the trench, it became increasingly recognized that (i) the nature of crustal rocks is important for the formation of these deposits, (ii) some of the mineral belts include deposits of widely different ages, and (iii) many deposits at a former plate margin formed long after subduction had ceased (e.g., Ishihara,1998; Seedorff et al., 2005; Sinclair, 2007; Richards, 2009; Sato, 2012). The latter point is important, as it highlights that the controlling factor for the formation of deposits is the nature of the material that can be melted, rather than the tectonic setting at the time of deposit formation (cf. Romer and Kroner, 2016).

Porphyry Cu, Mo, Au, W, and Sn deposits generally form in different tectonic settings and involve different source rocks (Seedorff et al., 2005; Sinclair, 2007). Typically, porphyry Cu (±Mo) deposits occur in subduction-related continental magmatic arc settings, such as the Andean porphyry Cu belt (Cooke, 2005) and the southwest North American porphyry Cu province (Barra et al., 2005). The ore-bearing magmas have calc-alkaline compositions (Barra et al., 2005), a high oxidation state (ΔFMQ + 2; Jugo, 2009), and high volatile concentrations (i.e., H_2O, S,

☆ This article is part of a special issue entitled: 'Cu-Au West China (Zhiming Yang)' published in Ore Geology Reviews.

* Corresponding author.
E-mail address: lycyndd@163.com (W. Li).

https://doi.org/10.1016/j.oregeorev.2025.106584
Received 14 March 2024; Received in revised form 21 March 2025; Accepted 23 March 2025
Available online 24 March 2025

and Cl; Richards, 2011). They are derived from the partial melting of the metasomatized mantle with variable, but generally minor contributions of subducted sediments (Richards, 2011). Porphyry Mo (±Cu) deposits are chemically more diverse than porphyry Cu (±Mo) deposits and typically have higher contributions from crustal rocks. There are two major types of porphyry Mo (± Cu) deposits, the Climax- and Endako-types (Sinclair, 2007). Climax-type Mo deposits generally occur in rift settings, comparable to the Colorado Mineral Belt of western North America (Audétat and Li, 2017) and the Mo deposits in the Qinling–Dabie Orogen (Chen et al., 2017). These deposits are closely associated with fluorine-rich (>0.2 wt% F), highly evolved alkalic magmas (Zhang and Audétat, 2017) derived from the lithospheric mantle with variable input of material from the continental crust (Ludington and Plumlee, 2009). Endako-type Mo deposits, such as those of central British Columbia, are related to subduction zones (Sinclair, 2007). This type of deposit is related to fluorine-poor (<0. 2 wt% F) calc-alkaline magmas (Ludington and Plumlee, 2009) that derived from the remelting of juvenile arc crust with minor contributions from the depleted mantle (Whalen et al., 2001). Porphyry Cu—Au and Au deposits, such as the porphyry Cu—Au deposits in British Columbia (Devine et al., 2014) and Tibet (Xu et al., 2017; Lin et al., 2019) and the porphyry Au deposit in the western Yangtze craton, China (Li et al., 2016), may form in continental arc, island arc, and intracontinental extensional settings (Hou et al., 2017). These deposits are generally related to relatively oxidized and H_2O-rich calc-alkaline to shoshonitic magmas (Sinclair, 2007) that are derived from the partial melting of a thickened lower crust with variable contributions of melts from the lithospheric mantle (Yang et al., 2015; Wang et al., 2018; Bao et al., 2023). Porphyry W (±Mo) and Sn (±W) deposits are restricted to highly differentiated granitic rocks (Sinclair, 2007; Romer and Kroner, 2016). Porphyry W (±Mo) and porphyry Sn (±W) deposits occur in magmatic arc, continental collision, and intraplate extensional settings (Sinclair, 2007; Mao et al., 2017; Liu et al., 2020a,b). The ore-forming magmas predominately derive from the partial melting of the continental crust with variable, but generally minor contributions from the mantle (Romer and Kroner, 2016).

The Sanjiang Tethyan metallogenic domain hosts numerous porphyry- and/or granite-related Cu (—Mo), Cu—Au, Au, Mo (—Cu), W—Mo, and Sn—W deposits that fall in several age groups. Earlier studies mainly focused on the magmatic evolution and ore formation of individual deposits or particular types of deposits (Hou et al., 2007, 2015; Deng et al., 2014a, 2014b, 2017; Mao et al., 2019; Liu et al., 2020a,b; Yang and Cooke, 2019; Yang et al., 2020a,b; Wang et al., 2021a,b). Here, we want to stress that different types of deposits occur coevally in different segments of the same suture and that most deposits are not related with the closure of the Paleo-Tethys Ocean, but with the reactivation of this old suture during later collisions along the Meso-Tethys and Neo-Tethys sutures. For this purpose, we compile age, chemistry, and isotope (whole-rock Sr, Nd, and Pb and zircon Hf and O) data of intrusions and related deposits from the Paleo-Tethys, Meso-Tethys, and Neo-Tethys sutures of southwestern China (Fig. 1). Our compilation demonstrates (i) that mineralization is not strictly related to the closure of the oceanic tracts of the various Tethys branches, but to the tectonic reactivation of these sutures during the closure of neighboring oceanic tracts and (ii) that mineralization involves contrasting portions of mantle and crustal sources. The metal association of the deposits is controlled by the nature of the source rocks, which is related to the geological development before the suture formed. As deposits of different metal associations formed in the same segment of the suture, but at different times and different tectonic settings, we argue that the local tectonic setting during later reactivation of the suture determines which source rocks become available for melting and, thus, which type of mineralization may form.

2. Tectonic evolution and metallogenic framework along Tethys sutures of southern Asia

2.1. A brief history of Tethys oceans (from subduction to continental collision) in Asia

Tethys is a giant and long-lived oceanic system between Gondwana to the south and Laurasia to the north. Different branches of the Tethys were closed during Paleozoic–Mesozoic accretion and Cenozoic collision of Gondwana-derived fragments with Laurasia and Eurasia (Hou and Zhang, 2015; Metcalfe, 2013; Richards, 2015). Four major Tethyan oceans are identified in Asia, i.e., the Proto-Tethys Ocean (late Proterozoic to Silurian; Zhao et al., 2017; Liu et al., 2020a,b), the Paleo-Tethys Ocean (middle Devonian to late Triassic; Kapp et al., 2003; Xu

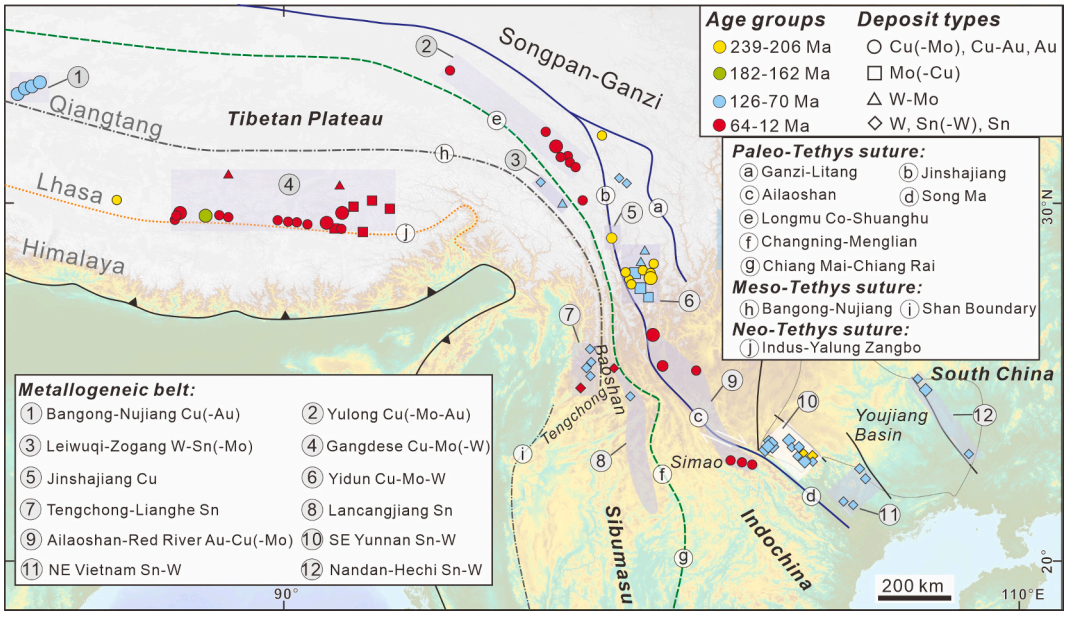

Fig. 1. Topographic map of southwestern China and adjacent areas showing major Tethys sutures and the distribution of Triassic to Tertiary Cu, Au, Mo, W, and Sn mineral belts in the eastern Tethyan domain. Age groups of mineral deposits are coded by different colors and main ore elements are coded by different symbol shapes.

et al., 2019), the Meso-Tethys Ocean (middle Permian to late Cretaceous; Xu et al., 2014), and Neo-Tethys Ocean (Jurassic to Cretaceous; Zhu et al., 2011; Metcalfe, 2013). The long-lived Proto-Tethys opened in the late Proterozoic and became closed in the Silurian with the collision of major Asian blocks with Gondwana (Zhao et al., 2017). After the closure of the Proto-Tethys Ocean, plate reorganization resulted in the fragmentation of eastern Gondwana. The Paleo-Tethys Ocean (Fig. 1; e.g., Longmu Co–Shuanghu, Changning–Menglian, Ganzi–Litang, Jinshajiang, and Ailaoshan) opened in the Devonian and was closed in the early Late Triassic (Metcalfe, 2021). The Bangong–Nujiang Meso-Tethys Ocean (Fig. 1) opened in the middle Permian and was closed in the late Cretaceous by subduction beneath the Lhasa and Qiangtang terranes (Shi et al., 2022). The Indus–Yarlung Zangbo Neo-Tethys Ocean (Fig. 1) opened in the late Triassic (Zhu et al., 2011; Metcalfe 2013) and was closed after the early Cretaceous Qiangtang–Lhasa collision (Zhu et al., 2016). The subsequent Paleocene India–Asia collision eventually resulted in the formation of the Tibetan Plateau (Yin and Harrison, 2000).

The Sanjiang (i.e., Jinshajiang, Lancangjiang, and Nujiang) belt lies between the South China block to the southeast, the Songpan–Ganzi accretionary complex to the east, and the West Burma block to the west. The Sanjiang belt is bordered by several crustal blocks, including the Simao, Baoshan, Tengchong, northern Qiangtang, southern Qiangtang, and Lhasa blocks (Fig. 1; Deng et al., 2014b). The Sanjiang belt is part of the suture of the former Paleo-Tethys Ocean. It formed in the late Triassic (Wang et al., 2020a; Metcalfe, 2021). This margin was recurrently tectonically reactivated during later tectonic events including the closure of the Meso-Tethys and Neo-Tethys oceans, i.e., the accretion of the Gangdese arc to Asia as well as the collision of India with Asia that resulted in the Himalayan orogen, the uplift of Tibet, and the lateral escape of thickened Asian crust (Deng et al., 2017; Chen et al., 2019; Yang et al., 2021; Xu et al., 2022).

Three major suture zones occur in the eastern Tethyan Metallogenic Domain, i.e., the Jinshajiang Paleo-Tethys, Bangong–Nujiang Meso-Tethys, and Indus–Yarlung Zangbo Neo-Tethys suture zones. Several belts with porphyry Cu (—Mo), Cu—Au, Au, Mo (—Cu), and W (—Mo) and granite-related Sn (—W) deposits occur along these three suture zones (Fig. 1). Deposits related to porphyries and/or granites within these metallogenic belts fall into several age groups and had formed in different tectonic settings (Table 1). For characterization of individual deposits mentioned in the text see Supplementary Material 1.

2.2. Mineral belts along the Paleo-Tethys sutures

The Jinshajiang–Ailaoshan Paleo-Tethys suture hosts major ore deposits. There are six main mineral belts along this suture (Fig. 1), i.e., the Yulong porphyry Cu belt, the Jinshajiang porphyry–skarn Cu polymetallic belt, the Yidun porphyry–hydrothermal Cu—Mo (—W) belt, the Ailaoshan–Red River porphyry–skarn Au—Cu (—Mo) belt, the southeastern Yunnan (Gejiu–Bozhushan–Malipo) granite-related Sn—W belt, and the northeastern Vietnam granite-related Sn—W belt (Supplementary Material 1). The age of deposits within the various mineral belts differs. Porphyry Cu mineralization in the Yulong belt formed between 44 and 35 Ma (Yang et al., 2022), whereas porphyry–skarn Cu mineralization in the Jinshajiang belt is 239 to 223 Ma old (Zhu et al., 2015; Li et al., 2021a). The Yidun belt hosts two age groups of mineralization, i.e., (i) 228–212 Ma porphyry Cu (—Mo) mineralization and (ii) 88–73 Ma porphyry–skarn Mo (—Cu) mineralization and 88–77 Ma porphyry-hydrothermal W—Mo mineralization (Chen et al., 2021; Leng et al., 2023; Li et al., 2011, 2017; Liu et al., 2016b; Yang et al., 2020b, 2023). The Ailaoshan–Red River belt has 36–34 Ma porphyry Cu (—Mo) and Cu—Au and 37–32 Ma porphyry Au mineralization (Table 1; Bao et al., 2023; Xu et al., 2023). The southeastern Yunnan mineral belt hosts at least three age groups of W mineralization (230–209 Ma, 151–142 Ma, and 92–88 Ma) and at least two age groups of Sn (—W) mineralization (230–220 Ma and 97–75 Ma; Table 1; Zhao et al., 2018; Cheng et al., 2019; Xu et al., 2022; Liu et al., 2023b; Zhao

Table 1
Age grouping of mineral deposits along the Paleo-, Meso-, and Neo-Tethys sutures.

Deposit type	Major deposits	Age (Ma)	Tectonic setting
1. Bangong-Nujiang Cu(−Au) belt			
Cu—Au	Duolong, Naruo	123–117	Subduction in magmatic arc
2. Yulong Cu(−Mo-Au) belt			
Cu(—Mo)	Yulong, Baomai	44–37	Strike-slip in intracontinental area
Cu—Au	Bada	35	Strike-slip in intracontinental area
3. Leiwuqi-Zogang W-Sn(−Mo) belt			
W—Mo	Larong	94–91	Post-collision extension in intracontinental area
W(—Sn)	Dongpulu	78	Post-collision extension in intracontinental area
4. Gangdese Cu(−Mo-W) belt			
Cu(—Mo)	Qulong, Jiama, Zhunuo	213–212, 49–48, 17–12	Subduction in magmatic arc, post-collision extension in intracontinental area
Cu—Au	Xiongcun	182–162	Subduction in magmatic arc
Mo(—Cu)	Bangpu, Tangbula	65–52, 32–15	Syn-collision in orogenic zone, post-collision extension in intracontinental area
W—Mo	Hahaigang, Jiagang	64–63, 19–18	Syn-collision in orogenic zone, post-collision extension in intracontinental area
5. Jinshajiang Cu polymetallic belt			
Cu	Yangla	239–223	Late- or post-collision in intracontinental area
6. Yidun Cu-Mo-W belt			
Cu(—Mo)	Pulang, Xuejiping	228–206	Subduction in magmatic arc
Mo(—Cu)	Tongchanggou	88–73	Post-collision in intracontinental area
W-Mo	Xiuwacu, Relin	88–77	Post-collision in intracontinental area
7. Tengchong-Lianghe Sn belt			
Sn	Tieyaoshan, Xiaolonghe, Lailishan	126–120, 76–70, 53–47	Subduction in magmatic arc, syn-collision in orogenic zone
8. Lancangjiang Sn belt			
Sn	Songshan, Tiechang	80–77, 32	Subduction in magmatic arc, strike-slip in intracontinental area
9. Ailaoshan-Red River Cu-Au(−Mo) belt			
Cu(—Mo)	Habo, Tongchang	36–34	Strike-slip in intracontinental area
Au	Beiya, Machangqing	37–32	Strike-slip in intracontinental area
10. Southeastern Yunnan Sn-W belt			
Sn(—W)	Gejiu, Dulong	97–75	Post-collision extension in intracontinental area
W	Nanwenhe, Guanfang	230–209, 145, 92–88	Post-collision extension in intracontinental area
11. Northeastern Vietnam Sn-W belt			
Sn(—W)	Alexandra	89–82	Post-collision extension in intracontinental area
W	Thien Ke	88–83	Post-collision extension in intracontinental area

(*continued on next page*)

Table 1 (*continued*)

Deposit type	Major deposits	Age (Ma)	Tectonic setting
12. Nandan-Hechi Sn-W belt			
Sn	Dachang,	99–89	Post-collision extension in intracontinental area
W	Damingshan	100–93	Post-collision extension in intracontinental area
Cu(—W)	Wangshe	94–93	Post-collision extension in intracontinental area

Age data are from Cao et al., 2019; Cheng and Mao, 2010; Gan et al., 2022; Liu et al., 2020a,b; Liu et al., 2023b; Mao et al., 2019; Nguyen et al., 2022; Sun et al., 2017, 2021; Yang et al., 2018, 2020b, 2022; Yang and Cooke, 2019; Zhen et al., 2021; Zhu et al., 2022.

Note, the Jiru deposit has two-stage Cu(—Mo) mineralization, i.e., Eocene formation and Miocene remobilization. Similarly, the Nanwenhe deposit shows two-stage W mineralization, i.e., Late Triassic deposit formation and Cretaceous W redistribution.

et al., 2024). The northeastern Vietnam belt has 89–82 Ma Sn (—W) and 88–83 Ma W mineralization (Nevolko et al., 2022; Nguyen et al., 2022). Note, there is another granite-related Sn—W belt bound to NW-trending fault zones parallel to the Ailaoshan–Songma suture, i.e., the Nandan–Hechi belt (Supplementary Material 1). This belt has 99–89 Ma Sn mineralization, 100–93 Ma W mineralization, and 94–93 Cu (—W) mineralization (Wang et al., 2019a; Gan et al., 2022). Furthermore, the Lancangjiang Sn belt along the Changning–Menglian suture (Fig. 1), another branch of the Paleo-Tethys, hosts two age groups of granite-related Sn mineralization (80–76 Ma and 33–32 Ma; Wang et al., 2024; Table 1; Supplementary Material 1). Only the Triassic deposits are related to the closure of the Paleo-Tethys. Most deposits, however, are much younger and, therefore, completely unrelated to the subduction processes that formed the Paleo-Tethys suture.

2.3. Mineral belts along the Meso-Tethys suture

There are two main mineral belts related to the Bangong–Nujiang Meso-Tethys suture (Fig. 1), i.e., the Bangong–Nujiang porphyry Cu (—Au) belt (Tang et al., 2021) and the Leiwuqi–Zogang granite-related W—Sn(—Mo) belt (Liu et al., 2020a,b; Supplementary Material 1). These belts host 123–117 Ma porphyry Cu—Au mineralization (Yang et al., 2020c), 94–91 Ma porphyry W—Mo mineralization, and 78 Ma granite-related W (—Sn) mineralization (Liu et al., 2020a,b, 2024) (Table 1). The older group of deposits is related to the subduction of the Meso-Tethys, whereas the younger groups of deposits postdate the closure of the Meso-Tethys and are related to post-collisional extension (Table 1).

2.4. Mineral belts along the Neo-Tethys suture

The Indus–Yarlung Zangbo Neo-Tethys suture (Fig. 1) hosts the Gangdese porphyry Cu belt and the Tengchong–Lianghe granite-related Sn belt (Supplementary Material 1). The Gangdese belt has multistage Cu—Mo—W mineralization, including 213–212 Ma porphyry Cu (—Mo) mineralization (Liu et al., 2023a), 182–162 Ma porphyry Cu—Au mineralization (Lang et al., 2019), 64–48 Ma porphyry Cu (—Mo), Mo (—Cu), and W—Mo mineralization, and 32–12 Ma porphyry Cu (—Mo) and Mo (—Cu) mineralization (Hu et al., 2015; Wang et al., 2020b; Sun et al., 2021; Hou et al., 2023; Shu et al., 2024; Yang and Cao, 2024). The Mesozoic deposits formed in magmatic arcs and are related to subduction processes, whereas the two age groups of Tertiary deposits are related to the collision of the Indian plate with Asia and post-collisional extension, respectively (Table 1). The Jiru porphyry Cu (—Mo) deposit shows two-stage Cu (—Mo) mineralization, Eocene formation and Miocene reactivation (Sun et al., 2021). The Tengchong–Lianghe belt is located between the Bangong–Nujiang Meso-Tethys and Indus–Yarlung Zangbo Neo-Tethys sutures and may connect with the eastern segment of the Gangdese belt (Fig. 1; Hou et al., 2007). At least three stages of granite-related Sn mineralization have been documented in this district (Table 1), i.e., early Cretaceous (126–120 Ma), late Cretaceous (76–70 Ma), and Eocene (53–47 Ma) Sn mineralization. Deposits of the oldest age groups are related to subduction and formed in an active magmatic arc, whereas deposits of the younger two age groups are coeval with collision after the closure of the Meso-Tethys Ocean (Fig. 1; Table 1).

3. Data base

3.1. Age of mineralization

The ages of Cu, Au, Mo, W, and Sn deposits related to porphyries and granites along the Paleo-, Meso-, and Neo-Tethys sutures are listed in Table S1 in Supplementary Material 2. Most porphyry- and/or granite-related Cu, Au, Mo, W, and Sn mineralization along the Jinshajiang–Ailaoshan and Changning–Menglian Paleo-Tethys, Bangong–Nujiang Meso-Tethys, and Indus–Yarlung Zangbo Neo-Tethys sutures fall in four age groups, i.e., 239–204 Ma, 182–162 Ma, 126–70 Ma, and 65–12 Ma (Fig. 1; Table 1). Each of these sutures hosts several generations of porphyry- and/or granite-related mineralization, which implies that not all deposits can be related to the formation of these sutures.

Along the Jinshajiang–Ailaoshan Paleo-Tethys suture (Fig. 1), there occur three major stages of mineralization with (i) late Triassic porphyry Cu (—Mo) deposits in the Yidun belt, late Triassic skarn Cu deposit in the Jinshajiang belt, and late Triassic W deposit in the southeastern Yunnan belt, (ii) late Cretaceous Mo—Cu and W—Mo deposits in the Yidun belt and late Cretaceous Sn—W deposits in the southeastern Yunnan belt and in the NW-trending fault zones parallel to the Ailaoshan suture, and (iii) Eocene porphyry Cu (—Mo) and porphyry Au deposits in the Ailaoshan–Red River belt. Similarly, there are at least two stages of Sn mineralization (late Cretaceous and Oligocene) along the Changning–Menglian suture.

The Bangong–Nujiang Meso-Tethys suture (Fig. 1) became closed in the early Cretaceous. There are two mineralization belts, the early Cretaceous Duolong porphyry Cu—Au belt and the late Cretaceous Leiwuqi–Zogang W—Mo—Sn—Pb—Zn belt. These two age groups of mineralization along the Meso-Tethys suture correspond to the younger two age groups of mineralization along the Paleo-Tethys suture, indicating that the formation of younger sutures reactivated older sutures and locally formed new mineralization along them.

Along the Indus–Yarlung Zangbo Neo-Tethys suture (Fig. 1), there is not only Cu, Mo, Au, W, and Sn mineralization related to the development of this suture, but also older mineralization related to magmatic arcs that were accreted along this suture. These older deposits include the late Triassic Luerma porphyry Cu deposit and the early to middle Jurassic Xiongcun porphyry Cu—Au belt in the western Gangdese belt. Deposits related to the closure of the Neo-Tethys Ocean include Miocene porphyry Cu deposits, Eocene and Miocene porphyry Mo deposits, Paleocene and Miocene porphyry W—Mo deposits in the eastern Gangdese Cu—Mo belt, as well as deposits of the late Cretaceous and Eocene Tengchong–Lianghe Sn belt in the southward extension of the Indus–Yarlung Zangbo Neo-Tethys suture.

3.2. Whole-rock major and trace element compositions

Whole-rock major and trace element compositions of porphyries and/or granites with related Cu, Au, Mo, W, and Sn deposits from the eastern Tethyan domain are shown in Table S2 in Supplementary Material 2. Intrusions related to porphyry Cu(—Mo), Cu—Au, Au, and Mo (—Cu) deposits are mainly granite porphyries, monzogranite porphyries, quartz diorite porphyries, and granodiorite porphyries (Fig. 2A; Table S2 in Supplementary Material 2). These porphyry intrusions commonly have high SiO_2 contents (59.8–75.7 wt%), high total alkali

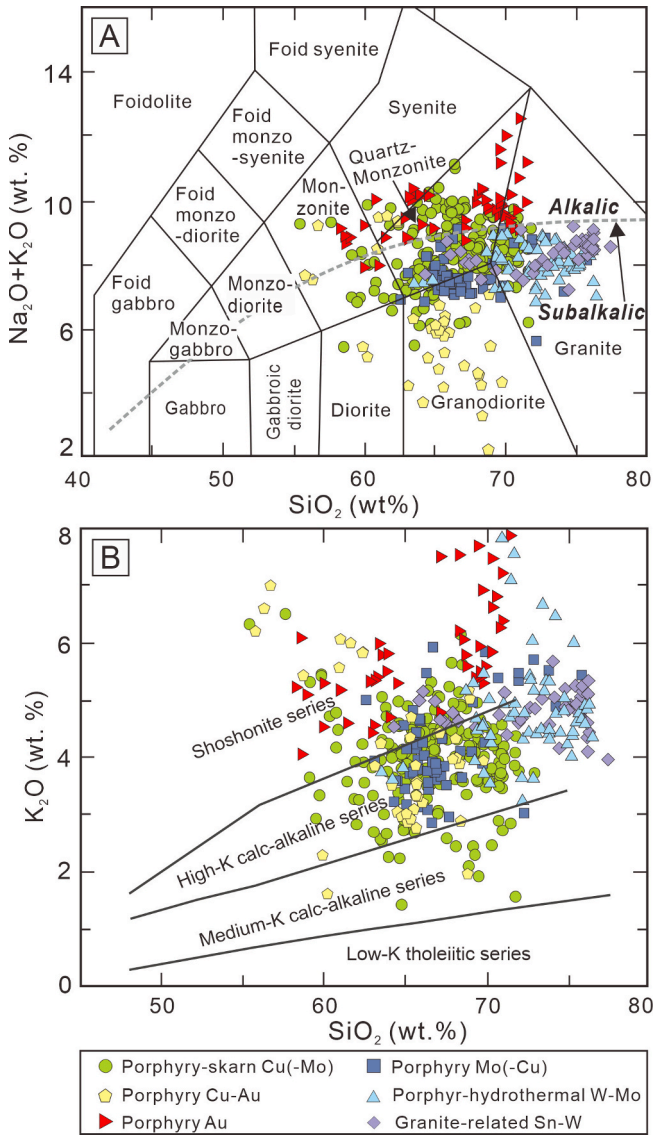

Fig. 2. Major element discrimination diagrams showing porphyry and granite intrusions with related Cu, Au, Mo, W, and Sn deposits from the eastern Tethyan domain. (A) (Na_2O + K_2O) vs. SiO_2 diagram (Middlemost, 1994). Porphyries with Cu (–Mo) and Au deposits fall in the range of monzonite, quartz monzonite, and granite, porphyries with Mo (–Cu) deposits fall in the range of quartz monzonite and granodiorite, whereas intrusions with Sn-W deposits are quartz monzonite and granite. (B) In the K_2O vs. SiO_2 diagram (Peccerillo and Taylor, 1976), intrusions with Cu (–Mo), Cu (–Au), Mo (–Cu), and Sn–W deposits fall in the fields of high-K calc-alkaline to shoshonite series, whereas intrusions with Au deposits belong to the shoshonite series. The chemical data for the deposits are from Cheng and Mao (2010), Chen et al. (2015), Wang et al. (2014a,b), Hu et al. (2015), Tang et al. (2015), Leng et al. (2018a,b), He et al. (2019), Huang et al. (2019), Liu et al. (2020a,b), Xu et al. (2020, 2022), Yang et al. (2009, 2020a), Guo et al. (2022 and references therein), Sun et al. (2017,2021), and Tian et al. (2022).

contents (Na_2O + K_2O = 6.08–12.50 wt%), relatively low aluminum saturation indexes (A/CNK = 0.79–1.32), weakly negative Eu anomalies (average Eu/Eu* ratio = 0.88), and high Sr/Y (average values > 60) and $(La/Sm)_N$ (average values > 5) ratios (Figs. 2, 3, and 5; Table S2 in Supplementary Material 2). These intrusions belong to weakly peraluminous to metaluminous, high-K calc-alkaline and shoshonite series (Fig. 2). Normalized to the average compositions of the Upper Continental Crust (UCC), these porphyry intrusions show significant enrichments of Cu and Mo (Fig. 4A). Relative to Primitive Mantle (PM), these

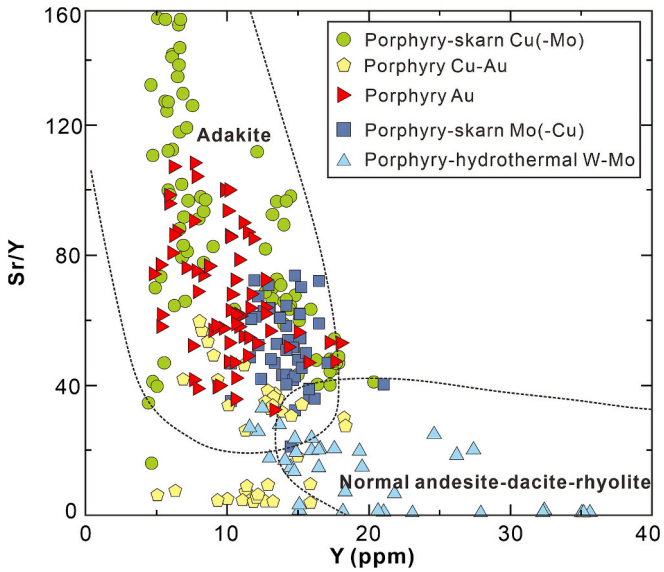

Fig. 3. Sr/Y vs. Y diagram for Cu, Au, Mo, W, and Sn deposits in the eastern Tethyan metallogenic domain. Porphyries with major Cu(–Mo), Au, and Mo (–Cu) deposits and porphyries with minor Cu–Au show adakite-like features, whereas porphyries and granites with W–Mo deposits have magmatic arc signatures. Data sources as in Fig. 2.

porphyry intrusions are enriched in large ion lithophile elements (LILEs, i.e., K, Rb, and Cs), as well as Th, U, and Pb, and depleted in Nb, Ta, Ti, and P (Fig. 4B).

In contrast, intrusions related to W—Mo and Sn—W deposits consist of monzogranite porphyries, monzogranites, and granites. These intrusions show relatively high SiO_2 contents (67.7–77.4 wt%), high total alkali contents (Na_2O + K_2O = 6.75–9.73 wt%), and relatively high aluminum saturation indexes (A/CNK = 0.94–1.66), moderately to strongly negative Eu anomalies (average Eu/Eu* ratio = 0.33), and low Sr/Y ratios (average values < 60) (Figs. 3 and 5; Table S2 in Supplementary Material 2). These intrusions primarily belong to peraluminous, high-K calc-alkaline series (Fig. 2B). Relative to UCC, W—Mo-bearing porphyries and granites are enriched in the ore elements W, Mo, and Sn and strongly depleted in Sr, Ba, and Eu, whereas granites related to Sn-W deposits are enriched in Sn and W and strongly depleted in Sr, Ba, and Eu (Fig. 4A). The Sn and W contents are positively correlated with increasing Rb/Sr ratios (Fig. 6). These granites are enriched in the alkali elements Li, Rb, and Cs, as well as the lithophile elements Be, U, and Th, and the chalcophile element Pb (Fig. 4).

3.3. Whole-rock Sr—Nd—Pb compositions

The whole-rock Sr, Nd, and Pb isotopic compositions of porphyries and/or granites with related Cu, Au, Mo, W, and Sn deposits from the eastern Tethyan domain are listed in Tables S3 and S4 in Supplementary Material 2. The ore-bearing intrusions from the various deposit types define on the εNd(t) vs. $^{87}Sr/^{86}Sr(t)$ diagram (Fig. 7A) a binary mixing trend between the endmembers Paleoproterozoic crust (εNd(t) = –11 to –15; two-stage model age of 1.8 to 2.1 Ga) and depleted mantle. Samples from the Jurassic Xiongcun Cu-Au deposits plot closest to the mantle endmember, whereas the various Sn-W deposits are dominated by the crustal endmember (Fig. 7A).

Intrusions with associated deposits of Cu, Au, and Mo are characterized by a broad range of εNd(t) values and a relatively narrow range of $^{87}Sr/^{86}Sr(t)$ values (Fig. 7A), reflecting variable contributions from the mantle and the Paleoproterozoic crust (Sun et al., 2021; Liu et al., 2023a; Xu et al., 2023). The crustal contribution to these I-type rocks may represent material that (i) was subducted to the mantle and metasomatized the lithospheric mantle that represents the sources of these I-

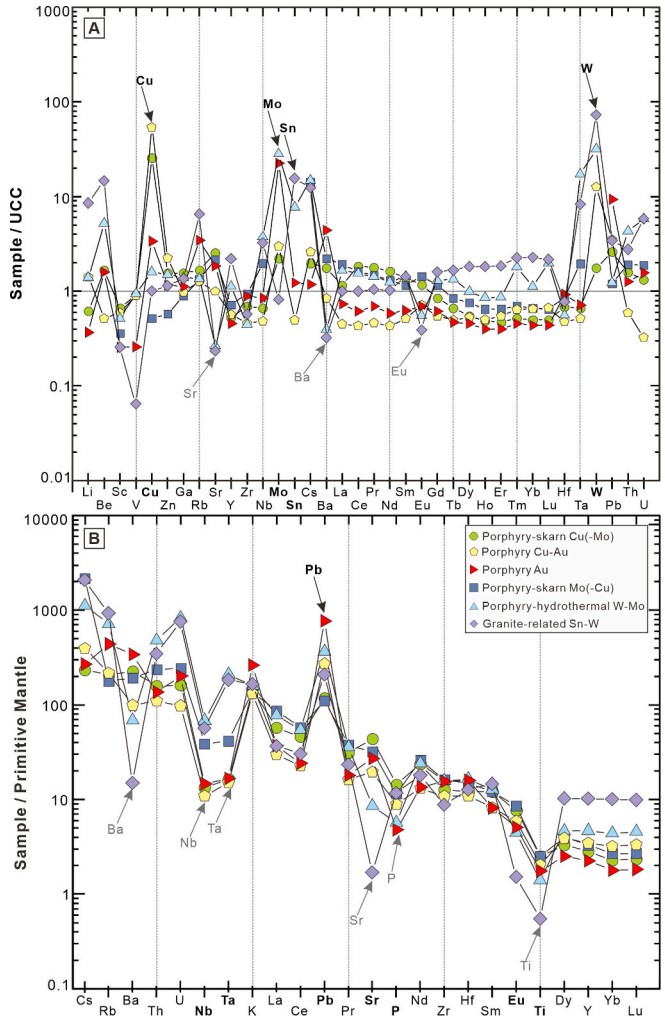

Fig. 4. Trace element contents normalized to the average compositions of Upper Continental Crust (UCC; Rudnick and Gao 2003) and Primitive Mantle (PM; McDonough and Sun, 1995). (A). Relative to the UCC, porphyry and granite with W–Mo and Sn–W deposits show much stronger negative anomalies for Sr, Ba, and Eu than porphyries with Cu (–Mo), Cu–Au, Au, and Mo (–Cu) deposits, indicating different sources and more intense fractionation. (B). Relative to the PM, all intrusions with Cu (–Mo), Cu–Au, Au, and Mo (–Cu) deposits have positive Pb and negative Nb, Ta, and Ti anomalies. These anomalies, which are differently intense for the various types of mineral deposits are hallmark fingerprints (along with high contents of Li and Rb) for the involvement of crustal material in subduction-related magmatic rocks, respectively. Data sources as in Fig. 2.

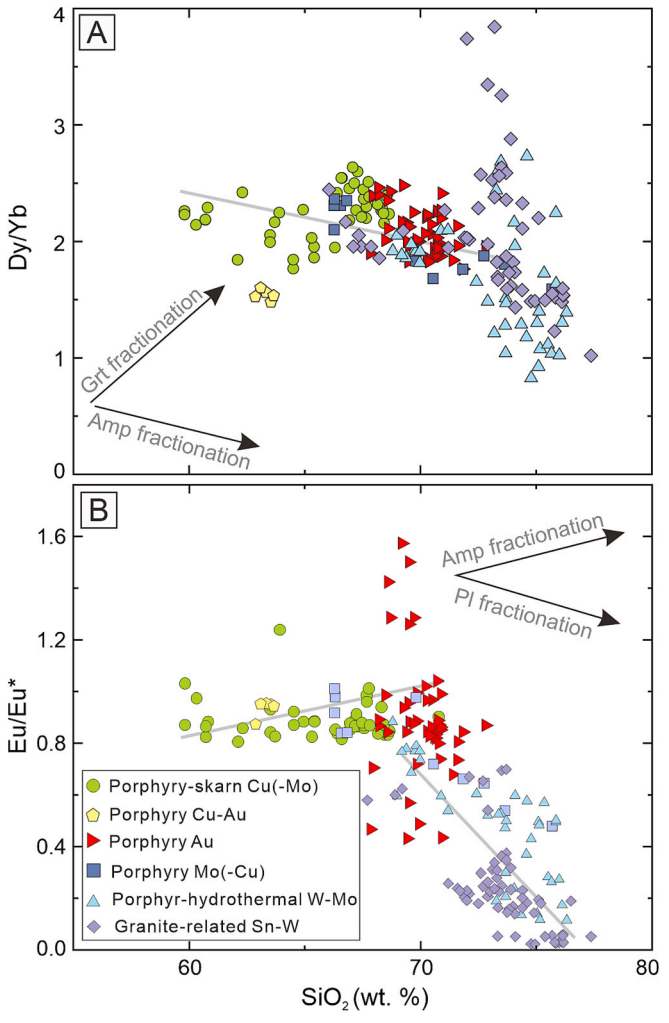

Fig. 5. (A) Dy/Yb and (B) Eu/Eu* ratios versus SiO_2 contents. The diagrams reflect that amphibole fractionation was important in porphyries and/or granites with Cu–Mo, Mo (–Cu), Au, and Cu–Au mineralization, whereas feldspar fractionation controlled the evolution of porphyry and/or granite intrusions with W–Mo and Sn–W mineralization. Data sources as in Fig. 2.

type rocks or (ii) was acquired during the passage of the mantle-derived melt through the crust by assimilation of wall rocks or by mixing with crustal melts. The Xiongcun Cu—Au deposit, located in the Gangdese arc, has high εNd(t) values (up to 6) and has little or no contributions from the crust. The syenite porphyry hosting the Eocene Yao'an Au-polymetallic deposit (Fig. S2 in Supplementary Material 1) has low whole-rock εNd(t) values (as low as –13; Yan et al., 2024), demonstrating that the source rocks are dominated by ancient continental crust (Fig. 7). The Yao'an Au-polymetallic deposit belongs to the same age group as the Beiya and Machangqing Au deposits near the Jinshajiang–Ailaoshan–Red River Paleo-Tethys suture, but is bound to a structure some 200 km farther to the east, within the Yangtze craton, which may account for the low εNd(t) values (Fig. S2 in Supplementary Material 1).

Late Cretaceous and Cenozoic W—Mo and Late Cretaceous and Paleogene Sn—W mineralization is characterized by low εNd(t) values (down to –12, corresponding to a two-stage model age of 1.9 Ga) and variable, but generally very radiogenic $^{87}Sr/^{86}Sr(t)$ values (Fig. 7A). The low εNd(t) values demonstrate that these rocks are dominated by ancient crustal material. The very high $^{87}Sr/^{86}Sr(t)$ values of some samples imply that the source rocks of these crustal melts also had very high $^{87}Rb/^{86}Sr$ values, such as feldspar- and carbonate-poor shales. Feldspar and carbonates are major hosts of Sr in sedimentary rocks. The decomposition of these minerals results in Sr loss, whereas the formation of clay minerals results in the concentration of Rb. Both processes lead to high Rb/Sr ratios in the sediments and, thus, produce with increasing age high $^{87}Sr/^{86}Sr$ values. Thus, the Sr—Nd isotope compositions of intrusions with W—Mo, Sn—W, and Sn deposits are compatible with the partial melting of metasedimentary rocks derived from ancient, intensely weathered crust (cf. Romer and Kroner 2022).

The Pb isotope compositions of sulfides from porphyry Cu (—Mo), Cu (—Au), Au, and Mo (—Cu) deposits define several scattered, sub-parallel fields on the $^{207}Pb/^{204}Pb$ vs. $^{206}Pb/^{204}Pb$ diagram, which essentially correspond to the various age groups (Fig. 9). Each trend represents a binary mixture between mantle Pb and ancient crustal Pb. As crustal rocks have higher Pb contents than mantle rocks (Rudnick and Gao, 2003) already minor contributions of crustal material shift the Pb isotope compositions toward the upper continental crust curve (UC in Fig. 9; Zartman and Doe, 1981). Lead of the porphyry- and/or granite-

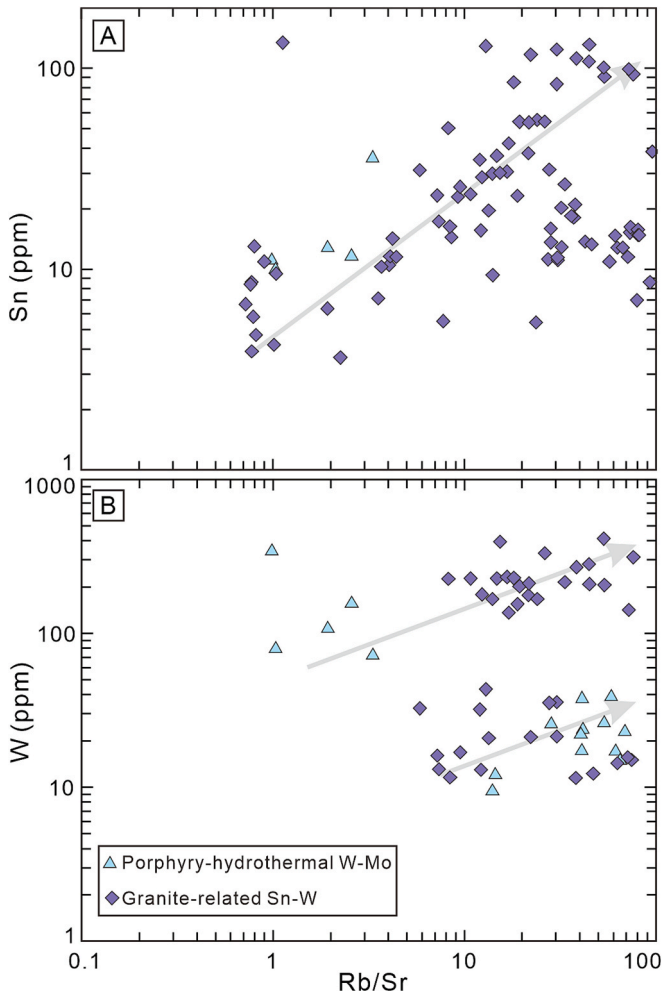

Fig. 6. (A) Tin and (B) W contents versus Rb/Sr ratios (modified after Romer and Kroner, 2016). The diagrams show the increase of Sn and W contents during magmatic fractionation. Note, the increase of W contents follows two separate fractionation trends. Data sources as in Fig. 2.

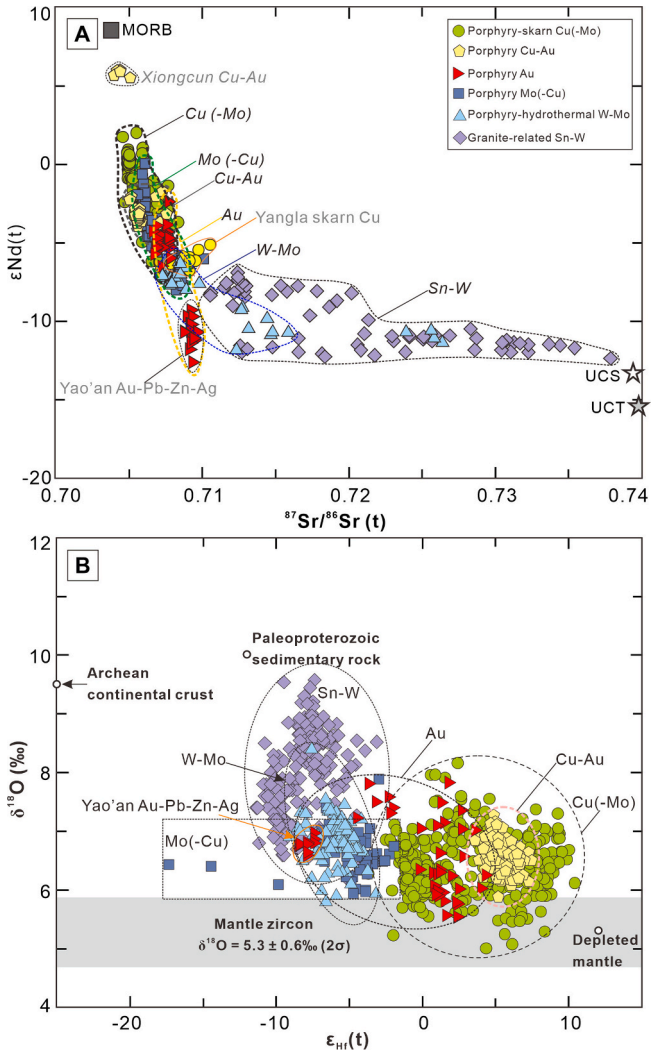

Fig. 7. (A) εNd(t) versus $^{87}Sr/^{86}Sr(t)$ diagram for the Cu, Au, Mo, W, and Sn deposits shown in Fig. 1 (except for the Hahaigang, Dongpulu, Xinzhai, Nanwenhe, Tiechang, Songshan, Thienke, and NuiPhao deposits for which no Sr–Nd isotope data are available). The binary mixing trend reflects contributions from the mantle and Paleoproterozoic crust (or younger sediments derived from the Paleoproterozoic crust). of Sr–Nd isotope data as in Fig. 2. Strontium–Nd isotope data for crust and mantle end members are from: Xigeza (Indus–Yarlung Zangbo) Neo-Tethyan ophiolite (MORB; Xu and Castillo, 2004); Late Triassic Darongshan S-type granites in South China (UCS; Qi et al., 2007); and strongly peraluminous granite in Tibet (UCT; Zhu et al., 2011). (B) Diagram of zircon εHf(t) vs. $\delta^{18}O$ (‰) data for the Cu, Au, Mo, W, and Sn deposits of the eastern Tethyan domain. Porphyry with Cu (–Mo) deposits have compositions that extend from the mantle field toward compositions reflecting some crustal additions. The compositional range represents contributions from melting of lithospheric mantle or subducted oceanic crust (high εHf(t) values) and crust (low εHf(t) values). Porphyries with Mo (–Cu) deposits seem to have higher crustal input than porphyries with Cu (–Mo) deposits. Granitoids with Sn–W deposits are dominantly derived from the partial melting of metasedimentary rocks. Sources of the Hf–O isotope data as in Fig. 2. End-members: depleted mantle (DM) has εHf(t) = 12 and $\delta^{18}O$ = 5.3 ‰; Paleoproterozoic supracrustal rocks have εHf(t) = –12 and $\delta^{18}O$ = 10 (Li et al., 2009); Archean continental crust has εHf(t) = 9.5 and $\delta^{18}O$ = –25 ‰ (Zhu et al., 2017).

related W—Mo and Sn—W deposits is mainly derived from ancient crust.

The Pb isotope data fall in the $^{208}Pb/^{204}Pb$ vs. $^{206}Pb/^{204}Pb$ diagram between the Pb evolution curves of upper continental crust and lower continental crust (UC and LC in Fig. 9; Zartman and Doe, 1981). As U and Pb are lost preferentially relative to Th during high-grade metamorphism, ancient lower crust commonly has high $^{208}Pb/^{204}Pb$ values at relatively low $^{206}Pb/^{204}Pb$ values (Zartman and Doe, 1981). Therefore, such Pb isotopic compositions commonly are interpreted to reflect partial melting or assimilation of ancient lower crustal rocks. The $^{208}Pb/^{204}Pb$ vs. $^{206}Pb/^{204}Pb$ diagram (Fig. 9), however, is ambiguous, as intense chemical weathering also results in the preferential loss of U and Pb relative to Th. Therefore, ancient sedimentary rocks may have similar Pb isotope signatures as high-grade metamorphic rocks even there was no ancient high-grade metamorphism (cf. Romer and Hahne 2010; Franz et al., 2013). It is important to note that time is essential for the development of these Pb isotope signatures. "Lower-crustal" Pb isotope signatures are mainly found in rocks that had experienced Archean and Early Proterozoic high-grade metamorphism or intense chemical weathering, but not rocks that had experienced geologically young high-grade metamorphism or weathering. Whereas the Pb isotope signature provides a fingerprint for the decoupling of U and Pb from Th, the Pb isotope signatures provide no constraints where these source rocks were when they melted. For the data shown in Fig. 9, we prefer the involvements of ancient deeply weathered sediments (or sedimentary rocks) rather than ancient lower crustal rocks, as high-grade metamorphism typically results in Rb loss relative to Sr (keeping $^{87}Sr/^{86}Sr(t)$ values low), whereas weathering typically results in Rb gain relative to Sr, which leads to high $^{87}Sr/^{86}Sr(t)$ values in the sedimentary rocks and explains the high $^{87}Sr/^{86}Sr(t)$ values of some intrusions.

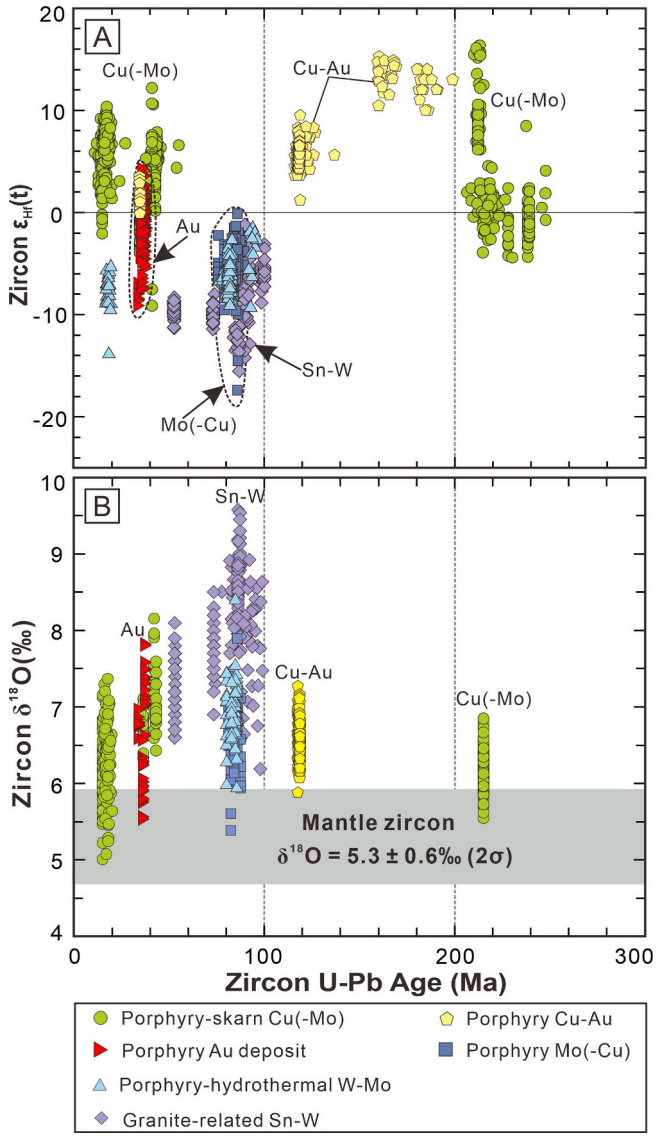

Fig. 8. Variation of the Hf and O isotopic compositions of zircon for different types of intrusions and ages. (A) Zircon εHf(t) vs. U–Pb age (Ma). Porphyry intrusions with Cu (–Mo) and Cu–Au deposits are sourced from the mantle or the juvenile crust, whereas porphyries and/or granites with Mo (–Cu), W–Mo, and Sn–W mineralization show significant contributions of ancient crust. (B) Zircon $\delta^{18}O$ (‰) vs. U-Pb age (Ma). Granites with Sn–W mineralization have higher zircon $\delta^{18}O$ values than other intrusions, reflecting larger contributions of sedimentary rocks to the melt. Data sources of Hf–O isotope data: Li et al. (2013), Wang et al. (2014a,b), Chen et al. (2015), Hu et al. (2015), Tang et al. (2015), Leng et al. (2018a,b), Huang et al. (2019), Liu et al. (2020a,b), Yang et al. (2020a, 2020b), Guo et al. (2022), and Xu et al. (2020, 2022).

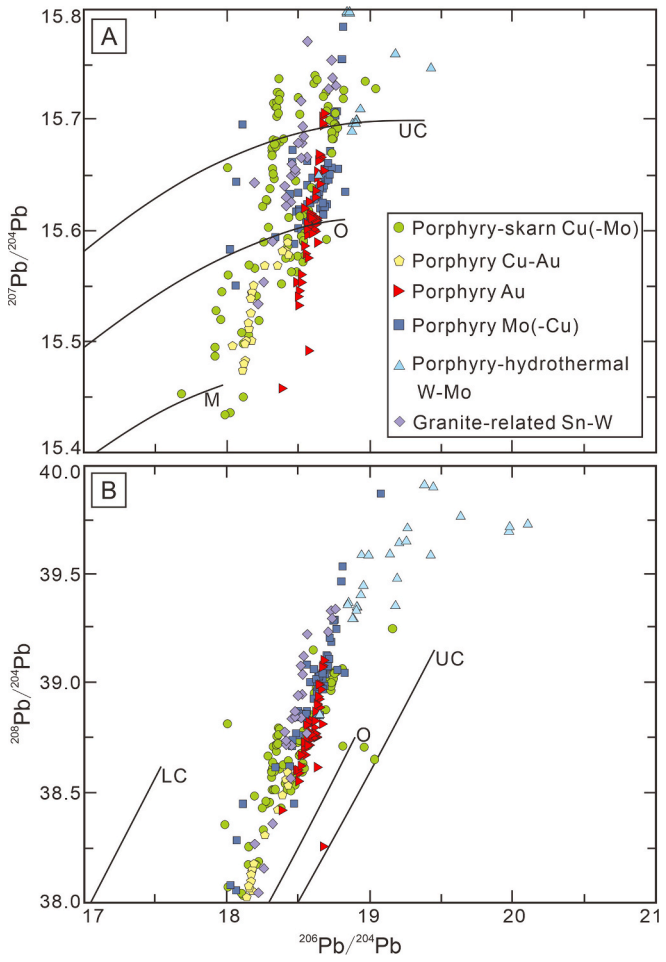

Fig. 9. Pb isotope ratios for sulfides from the Cu, Au, Mo, W, and Sn deposits of the eastern Tethyan domain. (A) In the $^{207}Pb/^{204}Pb$ vs. $^{206}Pb/^{204}Pb$ diagram, porphyry Cu(–Mo), Cu–Au, Au and Mo(–Cu) deposits fall between the evolution curves for Upper Continental Crust (UC) and Mantle (M; Zartman and Doe, 1981), porphyry and/or granite-related W–Mo and Sn–W deposits fall into a field near UC. (B) $^{208}Pb/^{204}Pb$ vs. $^{206}Pb/^{204}Pb$ diagram. Most data fall between the curves for the Upper Continental Crust (UC) and the Lower Continental Crust (LC; Zartman and Doe, 1981). Data sources: The Pb isotope compositions are from Cheng et al. (2012), Tang et al. (2015), Gao et al. (2017), Sun et al. (2017), Chen et al. (2018), Huang et al. (2019), Liu et al. (2016a,2020a,b), and Li et al. (2016, 2021a,b).

3.4. *In-situ zircon Hf—O compositions*

In-situ zircon Hf and O isotope compositions of porphyries and/or granites with related Cu, Au, Mo, W, and Sn deposits from the eastern Tethyan domain are listed in Table S5 in Supplementary Material 2. The εHf(t) and $\delta^{18}O$ systematic of zircon from porphyries and/or granites with Cu, Au, Mo, W, and Sn mineralization shows a similar bimodal trend between depleted mantle and Paleoproterozoic rocks (Fig. 7B). Most porphyry and granite intrusions with Cu and Au deposits have variably positive εHf(t) values, reflecting the importance of contributions from the mantle. In contrast, intrusions with Mo, W, and Sn deposits have negative εHf(t) values, reflecting the higher importance of crustal sources (Figs. 7B and 8; Wang et al., 2014a; He et al., 2019; Gao et al., 2021). Most Mo-W deposits have low $\delta^{18}O$ values, whereas W and Sn deposits have a broad range of $\delta^{18}O$ values that may be as high as $\delta^{18}O$ values of ancient continental sediments (Fig. 7B). Most notably, the Yao'an Au-polymetallic mineralization also has low zircon εHf(t) values (as low as –9) similar to Mo, W, and Sn deposits (Fig. 7B), reflecting major contributions from ancient crust.

3.5. *Oxidation state of magma*

Porphyries and granites with Cu (—Mo), Cu—Au, Au, Mo (—Cu), W—Mo, and Sn—W deposits have contrasting oxidation states (Sato, 2012; Richards, 2015). The oxidation state of granitic magmas is an essential factor to control which metals become concentrated during magma evolution and eventually may form an ore deposit (Blevin and Chappell, 1992). Copper, Au, and Mo mineralization are related to oxidized, magnetite-series granitoids, whereas W and Sn mineralization are related to relatively reduced, ilmenite-series granitoids (Ishihara, 1998). Therefore, the oxidation state of magma is widely used to evaluate its potential to form economic mineralization (Richards, 2015;

Wang et al., 2018; Bao et al., 2023; Miao et al., 2023; Wang and Zhang, 2025). The contrasting oxidation state of protoliths controls the mobilization of ore elements during partial melting (Sinclair 2007; Richards, 2015), affecting the nature of the restite phases (e.g., Wolf et al., 2018), and the enrichment of ore elements during fractional crystallization. Thus, the oxidation state of the protolith controls the regional distribution of different metals of porphyry- and/or granite-related deposits.

Oxidation state of magmas forming Cu, Au, Mo, W, and Sn deposits in the eastern Tethyan domain was calculated using the approach proposed by Loucks et al. (2020). For data sources see Table S6 in Supplementary Material 2. Porphyry Cu (—Mo) mineralization in the eastern Tethys are related to relatively oxidized magmas, with ΔFMQ ranging from 0 to 3.5 (mean = 1.8; Wang et al., 2014b; Lu et al., 2016; Sun et al., 2021, 2023). Porphyry Cu—Au and porphyry Au deposits have similar ΔFMQ values, with ΔFMQ ranging from 0.3 to 1.8 (mean 1.1) and from 0.1 to 4.5 (mean 1.7), respectively (Fig. 10; Xu et al., 2023). The three age groups of porphyry Mo mineralization are associated with slightly less oxidized magmas (ΔFMQ = 0.3–2.6, mean = 1.3; Fig. 10; He et al., 2019; Li et al., 2022). The relatively oxidized character of Cu—Mo—Au porphyry arc magmas are caused by slab-derived fluids and/or carbonates that oxidize the mantle (Richards, 2003, 2022; Meng et al., 2021; Wang et al., 2024). The high oxidation state of porphyry Cu—Mo—Au deposits in post-collisional settings are inherited from a mantle source that was modified by earlier subduction of oceanic crust (Xu et al., 2023). In the oxidized mantle, sulfur occurs as sulfate rather than sulfide (Jugo et al., 2010), which allows for mobilization and enrichment of Cu and Au in oxidized magmas.

In contrast, porphyry- and/or granite-related W—Mo mineralization and granite-related Sn—W mineralization are closely associated with relatively reduced magmas. Porphyry- and/or granite-related W—Mo mineralization have ΔFMQ values of –2.0 to 2.8 (mean 0.7; Fig. 10; Liu et al., 2020a,b; Xu et al., 2020; Li et al., 2022; Zhao et al., 2024a,b), whereas granitic magma with Sn–W mineralization have slightly lower ΔFMQ values (–2 to 2, mean 0.0; Fig. 10; Xu et al., 2022; Zhang et al., 2022b).

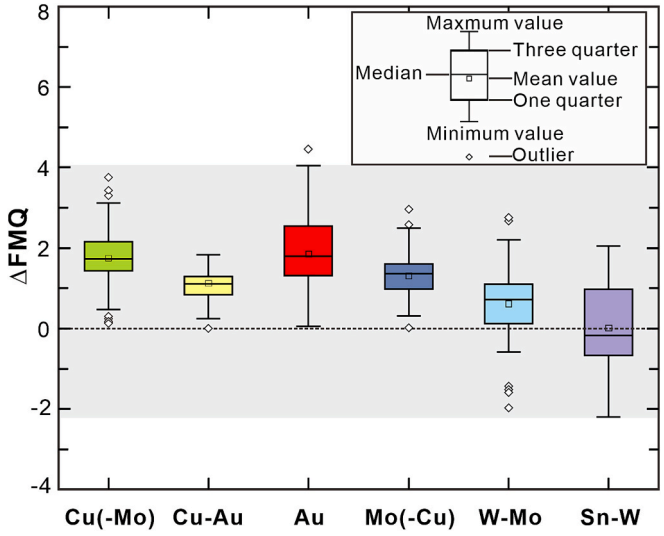

Fig. 10. Box diagram showing the oxidation state (ΔFMQ) of granites with Cu, Au, Mo, W, and Sn deposits in the eastern Tethyan domain. Porphyries with Cu (–Mo), Cu–Au, Au, and Mo (–Cu) deposits are relatively oxidized (mean ΔFMQ > 1), whereas porphyries and/or granites with W–Mo and Sn–W deposits are relatively reduced (mean ΔFMQ < 1). ΔFMQ calculated from zircon compositions using the method of Loucks et al. (2020). Zircon grains with La > 1 ppm and Ti > 20 ppm were excluded to avoid contaminations by apatite and titanite nano-inclusions (Miao et al., 2023). The trace element data of zircon for the deposits are from He et al. (2019), Liu et al. (2020a,b), Sun et al. (2021), Wang et al. (2021a,b), Zhang et al. (2022a,b), Xu et al. (2022, 2023), and Bao et al. (2023).

4. Discussion

4.1. Petrogenesis of ore-bearing porphyries and/or granites

The porphyries and/or granites with related mineralization of Cu, Au, Mo, W, and Sn show different compositions and their fractionation was dominated by different minerals (Supplementary Material 2; Figs. 4–6). Intrusions with Cu—Mo, Mo (—Cu), Au, and Cu—Au mineralization show adakitic (i.e., high Sr/Y) and I-type affinity (mainly Cu—Mo, Mo (—Cu), and Au), belonging to the high-K calc-alkaline and shoshonite series (Figs. 2 and 3). These porphyry intrusions are enriched in large ion lithophile elements (LILEs, i.e., K, Rb, and Cs), as well as Th, U, and Pb, and depleted in Nb, Ta, Ti, and P (Fig. 4). Negative Nb, Ta, and Ti anomalies and strongly positive Pb anomalies are typical for subduction-related magmatic rocks with additions from continental sediments that may have been subducted and modified the mantle source of these intrusions (Richards, 2003). Variable crustal contributions to the mantle source of the magmas are also shown by the Sr-Nd-Hf-O isotope compositions of porphyries with related Cu, Au, and Mo deposits (Fig. 7). The mantle-derived magmas evolved by fractional crystallization. The negative correlation between Dy/Yb and SiO_2 (Fig. 5A), the positive correlation between Eu/Eu* and SiO_2 (Fig. 5B), as well as the weak Eu anomalies (average Eu/Eu* ratio = 0.88; Table S2 in Supplementary Material 2) indicate that the REE budget of these rocks is controlled by amphibole fractionation (Davidson et al., 2007; Xu et al., 2015). The fractionation of amphibole raises the oxygen fugacity of the melt, which allows Cu, Mo, and Au to be concentrated in the residual magma, a crucial step for the formation of porphyry Cu(—Mo—Au) deposits (Zhang et al., 2022a).

Porphyry and/or granite intrusions with W—Mo and Sn—W mineralization have no Nb—Ta—Ti anomalies (Fig. 4B). These highly evolved granitic rocks belong to the calc-alkaline and high-K calc-alkaline series (Fig. 2B; Xu et al., 2020) and have high whole-rock $^{87}Sr/^{86}Sr(t)$ values, low whole-rock εNd(t) values, lower zircon εHf(t), and high $\delta^{18}O$ ratios (Fig. 7), which indicates that these rocks were dominantly derived from ancient crust or sediments derived from ancient crust. Intrusions of biotite granite and monzogranite with W—Mo and Sn mineralization have lower Ba, Sr, and Ti contents than porphyry intrusions with Cu—Mo, Mo (—Cu), Au, and Cu—Au mineralization (Fig. 4). Relative to UCC, W—Mo-bearing porphyries and granites are depleted in Sr, Ba, and Eu, which may represent a source signature (strongly chemically weathered feldspar-poor or feldspar-free sediments) and/or significant magmatic fractionation. Pronounced negative Sr, Ba, and Eu anomalies (average Eu/Eu* ratio = 0.33; Fig. 4; Table S2 in Supplementary Material 2) and negative correlation between Eu/Eu* and SiO_2 (Fig. 5B) indicate significant fractionation of feldspar during magmatic evolution. Feldspar fractionation also strongly increased the Rb/Sr ratios – a widely used fractionation index (e.g., Wai-Pan Ng et al., 2015; Zhang et al., 2020b) – of these intrusions (Fig. 6). The positive correlation of Sn and W contents with Rb/Sr (Fig. 6) indicates that extensive fractionation is important for the enrichment of Sn and W in melts.

4.2. Deposits related to the tectonic reactivation of the Paleo-Tethys suture

The Sanjiang belt hosts several Tethys sutures that are the traces after the closure of the Paleo-, Meso-, and Neo-Tethys oceans that had separated Gondwana-derived continental blocks (Metcalfe, 2021). In SE Asia, subduction and accretion leading to the closure of the Paleo-, Meso-, and Neo-Tethys oceans and subsequent continental collision took place in a broadly continuous way from the Late Paleozoic to Cenozoic (Deng et al., 2014a, 2017). The various sutures contain segments that were active margins and segments that were passive margins for most of their existence. These contrasting margin segments were juxtaposed

during initial accretion and collision and were reactivated during the collision of later arriving continental blocks in compressional, extensional, or strike-slip settings, largely depending on the orientation of the older suture to later plate movement (for analogues from Western Gondwana see Kroner et al., 2022). Mineralization of Cu, Au, Mo, W, and Sn along the Jinshajiang–Ailaoshan, Longmu Co–Shuanghu (–Lancangjiang), Bangong–Nujiang, and Indus–Yarlung Zangbo sutures predominantly falls in four age groups, i.e., 239–206 Ma, 182–162 Ma, 126–70 Ma, and 65–12 Ma (Table 1). The multistage remobilization of the various sutures resulted in the formation of several generations of porphyry- and granite-related mineralization within the various sutures, involving the same source rocks, i.e., the lithospheric mantle and sedimentary rocks from ancient continental crust. The nature of the predominant source rocks determines which metals may become concentrated in the magmatic rocks, whereas the tectonic setting and the regional and local stress fields determine whether major hydrothermal convection systems develop at the emplacement level of the magmatic rocks and whether mineral deposits may form.

The Triassic subduction and closure of the Paleo-Tethys Ocean resulted in the formation of porphyry Cu (—Mo) (228–206 Ma), skarn Cu (239–223 Ma), and skarn W–Sn deposits (230–209 Ma) along the Ganzi–Litang and Jinshajiang–Ailaoshan sutures (Fig. 1). The porphyry Cu (—Mo) deposits, such as the Pulang deposit in the Yidun terrane, formed in a subduction setting and are related to oxidized adakite-like porphyries that derived from the partial melting of the metasomatized mantle wedge (Leng et al., 2014). In contrast, the late Triassic Yangla skarn Cu deposit formed in a post-collisional setting, and differs from the porphyry Cu (—Mo) deposits by higher contributions of metasedimentary rocks (Fig. 7; Li et al., 2021b). Furthermore, the Late Triassic Xinzhai Sn and Nanwenhe W deposits in southeastern Yunnan mainly involve metasedimentary source rocks and possibly are related to regional metamorphism (Liu et al., 2023b).

The closure of the Bangong–Nujiang Meso-Tethys Ocean resulted in the formation of early Cretaceous Sn deposits in the Tengchong–Lianghe belt (Cao et al., 2016) and early Cretaceous porphyry Cu—Au mineralization (123–115 Ma) in the Duolong ore district (Fig. 1; Tang et al., 2021). Post-collisional extension induced large-scale Cretaceous magmatism with associated Mo—W—Sn (—Cu) mineralization in the Sanjiang and Tibet areas (Fig. 1), including porphyry–skarn Mo (—Cu) deposits (88–81 Ma), granite (porphyry)-related W—Mo (94–73 Ma), and 100–75 Ma Sn—W deposits (Fig. 1; Table 1). Late Cretaceous porphyry–skarn Mo (—Cu) and W—Mo deposits occur mainly in the northern Sanjiang area. Deposits of these two types are related to adakite-like I-type granite and highly fractionated granite, respectively (Li et al., 2017; Huang et al., 2019; Yang et al., 2020b). Coeval granite-related Sn—W deposits (Fig. 1 and Table 1) occur along the Bangong–Nujiang suture, and most importantly along the Ailaoshan suture (i.e., Gejiu, Bainiuchang, and Dulong ore clusters, SW China; Mao et al., 2019), NW-trending fault zones parallel to the Ailaoshan suture (i.e., Dachang and Damingshan ore clusters, SW China; Gan et al., 2022), and the Song Ma suture (i.e., PiaOac and Nui Phao–Tam Dao ore districts, NE Vietnam; Nguyen et al., 2022). Although the overall displacement along the Ailaoshan fault was sinistral, the multiply reactivated fault also experienced phases of dextral displacement (e.g., Roger et al., 2014). The deposits in the northern Sanjiang area formed in an extensional tectonic setting and involved contributions from the mantle (Wang et al., 2019b; Yang et al., 2020b). In contrast, coeval deposits along Ailaoshan and along faults parallel to the Ailaoshan fault (southern Sanjiang area) formed in strike-slip settings with local extensional domains (Fig. 10; Xu et al., 2022). These deposits derived from the partial melting of sedimentary rocks (Fig. 7). Mantle-derived magmas contributed little material to the granites in the southern Sanjiang area, but may have provided the heat to melt the metasedimentary rocks (Song et al., 2022).

The closure of the Neo-Tethys, culminating in the collision between India and Asia (ca. 65 Ma), resulted in contrasting mineralization styles in Tibet and the Sanjiang area. The India–Asia collision resulted in syn-collisional and post-collisional tectonics in southern Tibet, i.e., the Gangdese belt, and in large-scale NW-trending strike-slip faults and pull-apart basins (i.e., the Nangqen, Lanping, and Jianchuan; Hou et al., 2007) in the Sanjiang area. The different tectonic setting is reflected in contrasting mineralization with 64–12 Ma Cu—Mo—W deposits and 44–34 Ma Cu—Au (—Mo) deposits along the Indus–Yarlung Zangbo Neo-Tethys and Jinshajiang Paleo-Tethys sutures (Fig. 1; Table 1; Hou et al., 2015; Li et al., 2016) and 53–32 Ma Sn deposits along the Bangong–Nujiang and Changning–Menglian sutures (Fig. 1; Table 1; Chen et al., 2014; Zhu et al., 2022).

The reworking of Paleo-Tethys sutures during the closure of the Meso-Tethys and Neo-Tethys oceans and the India–Asia collision induced partial melting of crustal material with variable involvement of mantle melts and produced mineral deposits. The timing of the reactivation determined the age of magmatism, the nature of the source rocks determined the metal endowment of the intrusions (Fig. 7), and the local stress field around the intrusions determined whether metals were mobilized and redistributed from the intrusion by late-magmatic and external fluids to form mineral deposits (Fig. 11; Xu et al., 2022). The contrasting distribution of broadly coeval Cu, Au, Mo, W, and Sn deposits along differently oriented segments of the same suture (Figs. 1 and 11) indicates that the regional stress field, which depends on the orientation between different segments of the Paleo-Tethys suture and the plate movement, controls whether mantle-derived melts are emplaced in the upper crust where they may form deposits or remain in the lower crust where they may induce partial melting of the crust. At c. 90 Ma, the Sanjiang segment of the Paleo-Tethys suture was under extension (Wang et al., 2019b; Yang et al., 2020b) with Mo and Mo-W deposits, whereas the Ailaoshan segment was a strike-slip fault with Sn deposits in the Gejiu area (Fig. 11; Xu et al., 2022). Along different segments, the distribution of deposits is uneven. This is most obvious for the Gejiu area, where major granite-related deposits occur to the east of the Gejiu Fault, which strikes at a high angle to the Ailaoshan fault, but only minor deposits to the west (Fig. 11c). The Gejiu Fault separates domains with an extensional stress field at the time of granite emplacement to the east and domains with a compressional stress field to the west (cf. Jiang et al., 1997; Xu et al., 2022). Similarly, in the Sanjiang belt, major faults at high angle to the Paleo-Tethys suture separate segments of local extension and compression (Fig. 11b). Intrusions emplaced into extensional segments may produce significant deposits as the local stress field at the emplacement level, determines whether hydrothermal systems related to the porphyries and granites have a significant extent – and may produce deposit – or are only of small extent.

5. Conclusions

There are four major age groups of mineralization in the Sanjiang area that are spatially and genetically related to the formation and reactivation of Paleo-Tethys sutures, i.e., 239–206 Ma Cu (—Mo) and W (—Sn) mineralization; 182–162 Ma Cu—Au mineralization, 126–70 Ma Mo (—Cu), W—Mo, and Sn (—W) mineralization; and 53–32 Ma Cu (—Mo), Au, and Sn mineralization. Most of the deposits are not related to the development of the suture, but to its reactivation during later large-scale tectonic events. The various deposits formed during different tectonic processes (i.e., subduction, syn-collision, post-orogenic extension, and strike-slip movements) and mainly differ in the relative contributions of mantle and crustal sources. The nature of porphyry- and/or granite-related deposits is controlled by the relative contributions of mantle and crustal sources. During reactivations of the Paleo-Tethys suture, different deposit types formed along differently oriented segments of the suture, indicating that the relation between crustal-scale structures and the regional stress field controls whether mantle-derived melts (that may form Cu, Au, and Mo deposits) are emplaced into the upper crust or are emplaced into the lower crust where they cause partial melting of sedimentary rocks. These crustal melts may

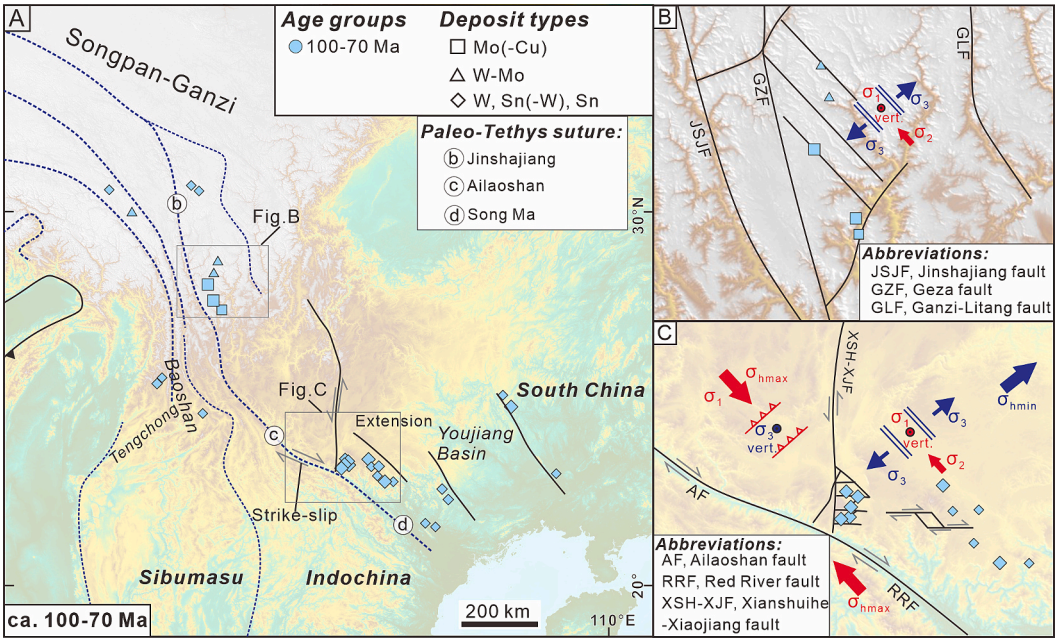

Fig. 11. (A) Topographic map shows the contrasting distribution of porphyry-/granite-related late Cretaceous (ca. 100–70 Ma) mineralization along the Jinshajinag–Ailaoshan–Red River Paleo-Tethys suture. (B) In the late Cretaceous extension setting, sigma 3 is horizontally oriented allowing for vertical fluid escape. The NW-trending faults provided efficient fluid pathways that ultimately resulted in Cu–Mo–W mineralization in the porphyries and granites and their contact zones with country rocks in the southern Yidun terrane. (C) The sinistral strike-slip Gejiu fault and dextral Ailaoshan–Red River fault zone form a Late Cretaceous conjugate fault system. The fault system is responsible for differences of the regional stress field and controls the distribution of granite-related Sn–W mineralization in southeastern Yunnan. To the west of the Gejiu fault (XSH-XJF), a vertically oriented σ3 favor the formation of horizontal tension gashes during late-stage magmatic fluid migration. Such a fracture network does not favor large-scale fluid flow and redistribution of Sn. To the east of the Gejiu fault, σ_3 is horizontally oriented allowing for vertical fluid escape (Jiang et al., 1997; Xu et al., 2022). This strikingly contrasting orientation of σ_3 eventually accounts for extensive mineralization to the east of the Gejiu fault, both in the upper parts of the granites and in country rocks in the roof. Panel C is adapted from Xu et al. (2022).

produce Sn and W deposits. At the emplacement level, the relation between major faults and the local stress field controls the circulation of magmatic and crustal fluids driven by the heat of the intrusion. Along extensional segments of major faults, hydrothermal convection cells may be large and form major deposits, whereas compressional segments of the same fault carry only minor mineralization as the convection cells are small. Therefore, major deposits may cluster in extensional segments of the reactivated suture.

Declaration of competing interest

The authors declare that they have no known competing financial interests or personal relationships that could have appeared to influence the work reported in this paper.

Acknowledgments

We are grateful to U Kroner for valuable discussion on tectonic setting and mineral deposits. We thank chief editor Huayong Chen, Dr. Chao Yang, and four anonymous reviewers for their helpful comments. This research was supported by the National Science and Technology Major Project of China (2024ZD1001702), the Major Scientific and Technological Projects in Yunnan Province (202202AG050006), the Selection Project of High-level Scientific and Technological Talents and Innovative Teams Project in Yunnan Province (202305AT350004 and 202205AS350015), the National Key R&D Program of China (2021YFC2901803), the National Natural Science Foundation of China (92055314), and a CSC student scholarship (202106400049).

Appendix A. Supplementary data

Supplementary data to this article can be found online at https://doi.org/10.1016/j.oregeorev.2025.106584.

Data availability

Data will be made available on request.

References

Audétat, A., Li, W., 2017. The genesis of Climax-type porphyry Mo deposits: Insights from fluid inclusions and melt inclusions. Ore Geol. Rev. 88, 436–460.
Bao, X.S., He, W.Y., Mao, J.W., Liang, T., Wang, H., Zhou, Y.M., Wang, J.J., 2023. Redox states and genesis of Cu- and Au-mineralized granite porphyries in the Jinshajiang Cu–Au metallogenic belt, SW China: studies on the zircon chemistry. Miner. Deposita 58, 1123–1142.
Barra, F., Ruiz, J., Valencia, V.A., Ochoa-Landín, L., Chesley, J.T., Zurcher, L., 2005. Laramide porphyry Cu-Mo mineralization in northern Mexico: Age constraints from Re-Os geochronology in molybdenite. Econ. Geol. 100, 1605–1616.
Blevin, P.L., Chappell, B.W., 1992. The role of magma sources, oxidation states and fractionation in determining the granite metallogeny of eastern Australia. Earth Environmental Science Transactions of the Royal Society of Edinburgh 83, 305–316.
Cao, H.W., Zhang, Y.H., Tang, L., Hollis, S.P., Zhang, S.T., Pei, Q.M., Yang, C., Zhu, X.S., 2019. Geochemistry, zircon U–Pb geochronology and Hf isotopes of Jurassic-Cretaceous granites in the Tengchong terrane, SW China: implications for the Mesozoic tectono-magmatic evolution of the Eastern Tethyan Tectonic Domain. Int. Geol. Rev. 61, 257–279.
Cao, H.-W., Zou, H., Zhang, Y.-H., Zhang, S.-T., Zheng, L., Zhang, L.-K., Tang, L., Pei, Q.-M., 2016. Late Cretaceous magmatism and related metallogeny in the Tengchong area: Evidence from geochronological, isotopic and geochemical data from the Xiaolonghe Sn deposit, western Yunnan, China. Ore Geol. Rev. 78, 196–212.
Chen, X., Burg, J.P., Liu, J., Qi, Y., Fan, W., Wang, K., 2019. Multistage Remobilization of the Southwestern Margin of the South China Plate: Insights From Zircon U-Pb Geochronology and Hf Isotope of Granitic Rocks From the Yao Shan Complex, Southeastern Tibet Plateau. Tectonics 38, 621–640.
Chen, X.-C., Hu, R.-Z., Bi, X.-W., Li, H.-M., Lan, J.-B., Zhao, C.-H., Zhu, J.-J., 2014. Cassiterite LA-MC-ICP-MS U/Pb and muscovite $^{40}Ar/^{39}Ar$ dating of tin deposits in the Tengchong-Lianghe tin district, NW Yunnan, China. Miner. Deposita 49, 843–860.
Chen, X.-C., Hu, R.-Z., Bi, X.-W., Zhong, H., Lan, J.-B., Zhao, C.-H., Zhu, J.-J., 2015. Zircon U–Pb ages and Hf–O isotopes, and whole-rock Sr–Nd isotopes of the

Bozhushan granite, Yunnan province, SW China: Constraints on petrogenesis and tectonic setting. J. Asian Earth Sci. 99, 57–71.
Chen, X.L., Leng, C.B., Zou, S.H., Li, K.X., Zhang, L.J., 2021. Geochemical compositions of apatites from the Xuejiping and Disuga porphyries in Zhongdian arc: Implications for porphyry Cu mineralization. Ore Geol. Rev. 130.
Chen, Y.-J., Wang, P., Li, N., Yang, Y.-F., Pirajno, F., 2017. The collision-type porphyry Mo deposits in Dabie Shan, China. Ore Geol. Rev. 81, 405–430.
Chen, X.-C., Zhao, C.-H., Zhu, J.-J., Wang, X.-S., Cui, T., 2018. He, Ar, and S isotopic constraints on the relationship between A-type granites and tin mineralization: A case study of tin deposits in the Tengchong–Lianghe tin belt, southwest China. Ore Geol. Rev. 92, 416–429.
Cheng, Y.B., Mao, J.W., 2010. Age and geochemistry of granites in Gejiu area, Yunnan province, SW China: Constraints on their petrogenesis and tectonic setting. Lithos 120, 258–276.
Cheng, Y., Mao, J., Rusk, B., Yang, Z., 2012. Geology and genesis of Kafang Cu–Sn deposit, Gejiu district, SW China. Ore Geol. Rev. 48, 180–196.
Cheng, Y., Spandler, C., Kemp, A., Mao, J., Rusk, B., Hu, Y., Blake, K., 2019. Controls on cassiterite (SnO2) crystallization: Evidence from cathodoluminescence, trace-element chemistry, and geochronology at the Gejiu Tin District. Am. Mineral. 104, 118–129.
Cooke, D.R., 2005. Giant Porphyry Deposits: Characteristics, Distribution, and Tectonic Controls. Econ. Geol. 100, 801–818.
Davidson, A., Turner, S., Handley, H., Macpherson, C., Dosseto, A., 2007. Amphibole "sponge" in arc crust? Geology 35, 787–790.
Deng, J., Wang, Q.F., Li, G.J., Li, C.S., Wang, C.M., 2014a. Tethys tectonic evolution and its bearing on the distribution of important mineral deposits in the Sanjiang region, SW China. Gondw. Res. 26, 419–437.
Deng, J., Wang, Q.F., Li, G.J., Santosh, M., 2014b. Cenozoic tectono-magmatic and metallogenic processes in the Sanjiang region, southwestern China. Earth Sci. Rev. 138, 268–299.
Deng, J., Wang, Q.F., Li, G.J., 2017. Tectonic evolution, superimposed orogeny, and composite metallogenic system in China. Gondw. Res. 50, 216–266.
Devine, F.A.M., Chamberlain, C.M., Davies, A.G.S., Friedman, R., Baxter, P., 2014. Geology and District-Scale Setting of Tilted Alkalic Porphyry Cu-Au Mineralization at the Lorraine Deposit, British Columbia. Econ. Geol. 109, 939–977.
Franz, L., Romer, R.L., de Capitani, C., 2013. Protoliths and phase petrology of whiteschists. Contrib. Miner. Petrol. 166, 255–274.
Gan, C.S., Wang, Y.J., Zhang, Y.Z., Qian, X., 2022. Petrogenesis of Late Cretaceous granites and implications for W-Sn mineralization in the Youjiang Basin, South China. Ore Geology Reviews 144, 104846.
Gao, X., Yang, L.-Q., Meng, J.-Y., Zhang, L.-J., 2017. Zircon U–Pb, molybdenite Re–Os geochronology and Sr–Nd–Pb–Hf–O–S isotopic constraints on the genesis of Relin Cu–Mo deposit in Zhongdian, Northwest Yunnan, China. Ore Geol. Rev. 91, 945–962.
Gao, X., Yang, L.-Q., He, W.-Y., Groves, D., 2021. Redox conditions, compositional parameters, and indirect subduction-related source of Cretaceous Sn and Cu–Mo fertile post-subduction granites in the Yidun Terrane of eastern Tibet. Ore Geol. Rev. 139, 104506.
Guo, J., Wu, K., Seltmann, R., Zhang, R., Ling, M., Li, C., Sun, W., 2022. Unraveling the link between mantle upwelling and formation of Sn-bearing granitic rocks in the world-class Dachang tin district, South China. GSA Bull. 134, 1043–1064.
He, J., Wang, B., Wang, L., Wang, Q., Yan, G., 2019. Geochemistry and geochronology of the Late Cretaceous Tongchanggou Mo–Cu deposit, Yidun Terrane, SE Tibet; implications for post-collisional metallogenesis. J. Asian Earth Sci. 172, 308–327.
Hou, Z.Q., Zaw, K., Pan, G.T., Mo, X.X., Xu, Q., Hu, Y.Z., Li, X.Z., 2007. Sanjiang Tethyan metallogenesis in S.W. China: Tectonic setting, metallogenic epochs and deposit types. Ore Geol. Rev. 31, 48–87.
Hou, Z.Q., Yang, Z.M., Lu, Y.J., Kemp, A., Zheng, Y.C., Li, Q.Y., Tang, J.X., Yang, Z.S., Duan, L.F., 2015. A genetic linkage between subduction- and collision-related porphyry Cu deposits in continental collision zones. Geology 43, 247–250.
Hou, Z.Q., Zhou, Y., Wang, R., Zheng, Y.C., He, W.Y., Zhao, M., Evans, N.J., Weinberg, R. F., 2017. Recycling of metal-fertilized lower continental crust: Origin of non-arc Au-rich porphyry deposits at cratonic edges. Geology 45, 563–566.
Hou, Z.Q., Wang, R., Zhang, H.J., Zheng, Y.C., Jin, S., Thybo, H., Weinberg, R.F., Xu, B., Yang, Z.M., Hao, A.-W., Gao, L., Zhang, L.T., 2023. Formation of giant copper deposits in Tibet driven by tearing of the subducted Indian plate. Earth Sci. Rev. 243, 104482.
Hou, Z.Q., Zhang, H.R., 2015. Geodynamics and metallogeny of the eastern Tethyan metallogenic domain. Ore Geol. Rev. 70, 346–384.
Hu, Y.-B., Liu, J.-Q., Ling, M.-X., Ding, W., Liu, Y., Zartman, R.E., Ma, X.-F., Liu, D.-Y., Zhang, C.-C., Sun, S.-J., Zhang, L.-P., Wu, K., Sun, W.-D., 2015. The formation of Qulong adakites and their relationship with porphyry copper deposit: Geochemical constraints. Lithos 220–223, 60–80.
Huang, M.-L., Bi, X.-W., Hu, R.-Z., Gao, J.-F., Xu, L.-L., Zhu, J.-J., Shang, L.-B., 2019. Geochemistry, in-situ Sr-Nd-Hf-O isotopes, and mineralogical constraints on origin and magmatic-hydrothermal evolution of the Yulong porphyry Cu Mo deposit, Eastern Tibet. Gondw. Res. 76, 98–114.
Ishihara, S., 1998. Granitoid Series and Mineralization in the Cricum–Pacific Granitic belts. Resour. Geol. 48, 219–224.
Jiang, Z.W., Oliver, N.H.S., Barr, T.D., Power, W.L., Ord, A., 1997. Numerical modeling of fault-controlled fluid flow in the genesis of tin deposits of the Malage Ore Field, Gejiu Mining District, China. Econ. Geol. 92, 228–247.
Jugo, P.J., 2009. Sulfur content at sulfide saturation in oxidized magmas. Geology 37, 415–418.
Jugo, P.J., Wilke, M., Botcharnikov, R.E., 2010. Sulfur K-edge XANES analysis of natural and synthetic basaltic glasses: Implications for S speciation and S content as function of oxygen fugacity. Geochim. Cosmochim. Acta 74, 5926–5938.
Kapp, P., Yin, A., Manning, C.E., Harrison, T.M., Taylor, M.H., Ding, L., 2003. Tectonic evolution of the early Mesozoic blueschist-bearing Qiangtang metamorphic belt, central Tibet. Tectonics 22, 1043.
Kroner, U., Stephan, T., Romer, R.L., 2022. Paleozoic orogenies and relative plate motions at the sutures of the Iapetus-Rheic Ocean. In: Kuiper, Y.D., Murphy, J.B., Nance, R.D., Strachan, R.A., Thompson, M.D. (Eds.), New Developments in the Appalachian-Caledonian-Variscan Orogen. Geological Society of America, Special Paper, pp. 1–23.
Lang, X.H., Wang, X.H., Deng, Y.L., Tang, J.X., Xie, F.W., Yang, Z.Y., Yin, Q., Jiang, K., 2019. Hydrothermal evolution and ore precipitation of the No. 2 porphyry Cu–Au deposit in the Xiongcun district, Tibet: Evidence from cathodoluminescence, fluid inclusions, and isotopes. Ore Geol. Rev. 114, 103141.
Leng, C.-B., Cooke, D.R., Hou, Z.-Q., Evans, N.J., Zhang, X.-C., Chen, W.T., Danišík, M., McInnes, B.I.A., Yang, J.-H., 2018b. Quantifying Exhumation at the Giant Pulang Porphyry Cu-Au Deposit Using U-Pb-He Dating. Econ. Geol. 113, 1077–1092.
Leng, C.B., Huang, Q.Y., Zhang, X.C., Wang, S.X., Zhong, H., Hu, R.Z., Bi, X.W., Zhu, J.J., Wang, X.S., 2014. Petrogenesis of the Late Triassic volcanic rocks in the Southern Yidun arc, SW China. Lithos 190–191, 363–382.
Leng, C.B., Gao, J.F., Chen, W.T., Zhang, X.C., Tian, Z.D., Guo, J.H., 2018a. Platinum-group elements, zircon Hf-O isotopes, and mineralogical constraints on magmatic evolution of the Pulang porphyry Cu-Au system, SW China. Gondw. Res. 62, 163–177.
Leng, C.-B., Wang, D.-Z., Yu, H.-J., Tian, F., Zhang, X.-C., 2023. Mapping hydrothermal alteration zones with short wavelength infrared (SWIR) spectra and magnetic susceptibility at the Pulang porphyry Cu-Au deposit, Yunnan, SW China. Miner. Deposita 59, 699–716.
Li, X.H., Li, W.X., Wang, X.C., Li, Q.L., Liu, Y., Tang, G.Q., 2009. Role of mantle-derived magma in genesis of early Yanshanian granites in the Nanling Range, South China: in situ zircon Hf-O isotopic constraints. Sci. China Ser. D Earth Sci. 52, 1262–1278.
Li, S.K., Liu, X.L., Lu, Y.X., Zhang, S.T., Liu, S.H., Chen, J.H., Li, Z.H., Yu, H.J., Zhang, C. Y., 2022. Indication of zircon oxygen fugacity to different mineralization control factors of porphyry deposits in Zhongdian ore-concentrated area, Southern Yidun Arc. Earth Sci. 47, 1435–1458 in Chinese with English abstract.
Li, W.-C., Pan, G.-T., Zhang, X.-F., Wang, L.-Q., Zhou, J.-X., 2021b. Tectonic evolution and multi–episodic metallogenesis of the Sanjiang Paleo-Tethys multi-arc-basin-terrane system, SW Tibetan Plateau. J. Asian Earth Sci. 221, 104932.
Li, J.-X., Qin, K.-Z., Li, G.-M., Xiao, B., Zhao, J.-X., Cao, M.-J., Chen, L., 2013. Petrogenesis of ore-bearing porphyries from the Duolong porphyry Cu–Au deposit, central Tibet: Evidence from U–Pb geochronology, petrochemistry and Sr–Nd–Hf–O isotope characteristics. Lithos 160–161, 216–227.
Li, W.C., Wang, J.H., He, Z.H., Dou, S., 2016. Formation of Au-polymetallic ore deposits in alkaline porphyries at Beiya, Yunnan, Southwest China. Ore Geol. Rev. 73, 241–252.
Li, B., Wang, X., Tang, G., Liu, Y., Zou, G., 2021a. S-Pb isotopes and tectono-geochemistry of the Lunong ore block, Yangla large Cu deposit, SW China: Implications for mineral exploration. Ore Geol. Rev. 136, 104249.
Li, W.C., Zeng, P., Hou, Z., White, N.C., 2011. The Pulang Porphyry Copper Deposit and Associated Felsic Intrusions in Yunnan Province, Southwest China. Econ. Geol. 106, 79–92.
Li, W.C., Yu, H.J., Gao, X., Liu, X.L., Wang, J.H., 2017. Review of Mesozoic multiple magmatism and porphyry Cu–Mo (W) mineralization in the Yidun Arc, eastern Tibet Plateau. Ore Geol. Rev. 90, 795–812.
Lin, B., Tang, J., Chen, Y., Baker, M., Song, Y., Yang, H., Wang, Q., He, W., Liu, Z., 2019. Geology and geochronology of Naruo large porphyry-breccia Cu deposit in the Duolong district. Tibet. Gondwana Research 66, 168–182.
Liu, H., Huang, H.X., Li, G.M., Li, W.C., Zhang, L.K., Lan, S.S., Lü, M.H., Song, W.J., 2023a. Subduction-related Late Triassic Luerma porphyry copper deposit, western Gangdese, Tibet, China: Evidence from geology, geochemistry, and geochronology. Ore Geol. Rev. 154, 105253.
Liu, X.L., Li, W.C., Zhang, N., Lai, A.Q., Li, Z., Yang, F.C., 2016a. Metallogenic system of the Yanshanian porphyry Mo polymetallic deposit in the Xiangcheng-Lijiang suture zone, western margin of Yangtze block, SW China. Acta Petrol. Sin. 32, 2281–2302.
Liu, X.L., Li, W.C., Zhang, N., Yang, F.C., 2016b. Geochemistry and petrogenesis of Triassic mineralized porphyries in the Geza of the Sanjiang orogenic belt, southwestern China. Int. Geol. Rev. 59, 965–980.
Liu, J., Li, W.C., Zhu, X.P., Wang, B.D., Jiang, J.S., Liu, H.F., 2020b. Magmatic evolution and related W–Mo mineralization in the Larong deposit, eastern Tibet: Evidence from zircon U–Pb ages, geochemistry and Sr–Nd–Hf isotopes. Ore Geol. Rev. 120, 103411.
Liu, J., Li, W.C., Zhou, Q., Cao, H.W., Gao, S.B., Liu, H., Wang, Y.Y., 2024. Major types, spatio-temporal distribution, and metallogenesis of magmatism-related polymetallic deposits in the Bangonghu–Nujiang metallogenic belt, Tibet. Ore Geol. Rev. 167, 105983.
Liu, Y.B., Zhang, L.F., Santosh, M., Dong, G.C., Zhou, H.Y., Que, C.Y., Yang, C.X., 2023b. Multi–stage metallogeny in the southwestern part of South China, and paleotectonic and climatic implications: A high precision geochronologic study. Geosci. Front. 14, 101536.
Liu, Q., Zhao, G., Li, J., Yao, J., Han, Y., Wang, P., Tsunogae, T., 2020a. Provenance of early Paleozoic sedimentary rocks in the Altyn Tagh orogen: Insights into the paleoposition of the Tarim craton in northern Gondwana associated with final closure of the Proto–Tethys Ocean. GSA Bull. 133, 505–522.
Loucks, R.R., Fiorentini, M.L., Henríquez, G.J., 2020. New Magmatic Oxybarometer Using Trace Elements in Zircon. J. Petrol. 61, egaa034.

Lu, Y.J., Loucks, R.R., Fiorentini, M.L., McCuaig, T.C., Evans, N.J., Yang, Z.M., Hou, Z.Q., Kirkland, C.L., Parra-Avila, L.A., Kobussen, A., 2016. Zircon Compositions as a pathfinder for Porphyry Cu± Mo± Au Deposits. Soc. Economic Geo. Spec. Pub. 19, 329–347.

Ludington, S., Plumlee, G.S., 2009. Climax-type porphyry molybdenum deposits. U.S. Geological Survey Open File report 2009-1215, 16.

Mao, J.W., Ouyang, H.G., Song, S.W., Santosh, M., Yuan, S.D., Zhou, Z.H., Zhang, W., Liu, H., Liu, P., Cheng, Y.B., Chen, M.H., 2019. Geology and Metallogeny of Tungsten and Tin deposits in China. Soc. Economic Geo. Spec. Pub. 22, 411–482.

Mao, J., Zhou, Y., Liu, H., Zhang, C., Fu, D., Liu, B., 2017. Metallogenic setting and ore genetic model for the Beiya porphyry-skarn polymetallic Au orefield, western Yunnan, China. Ore Geol. Rev. 86, 21–34.

McDonough, W.F., Sun, B.S.S., 1995. The composition of the Earth - ScienceDirect. Chem. Geol. 120, 223–253.

Meng, X.Y., Kleinsasser, J.M., Richards, J.P., Tapster, S.R., Jugo, P.J., Simon, A.C., Kontak, D.J., Robb, L., Bybee, G.M., Marsh, J.H., Stern, R.A., 2021. Oxidized sulfur-rich arc magmas formed porphyry Cu deposits by 1.88 Ga. Nat. Commun. 12, 2189.

Metcalfe, I., 2013. Gondwana dispersion and Asian accretion: Tectonic and palaeogeographic evolution of eastern Tethys. J. Asian Earth Sci. 66, 1–33.

Metcalfe, I., 2021. Multiple Tethyan ocean basins and orogenic belts in Asia. Gondw. Res. 100, 87–130.

Miao, X.B., Wang, R., Hou, Z.Q., Chang, Y.Z., Zhao, C.H., Ren, Y.Z., 2023. Mo endowment of porphyry deposits in the southern margin of the North China Craton controlled by magmatic water content. Miner. Deposita 58, 1499–1518.

Middlemost, E.A.K., 1994. Naming materials in the magma/igneous rock system. Earth Sci. Rev. 37, 215–224.

Mitchell, A.H.G., Garson, M.S., 1981. Mineral Deposits and Global Tectonic Settings. Academic Press, London, pp. 1–405.

Nevolko, P.A., Svetlitskaya, T.V., Nguyen, T.H., Pham, T.D., Fominykh, P.A., Tran, T.H., Tran, T.A., Shelepaev, R.A., 2022. Genesis of the Thien Ke tungsten deposit, Northeast Vietnam: Evidence from mineral composition, fluid inclusions, S-O isotope systematics and U-Pb zircon ages. Ore Geol. Rev. 143, 104791.

Nguyen, D., Wang, R., Yu, J., Wang, X.-L., Nguyen, Q., Pham, T., Do, V., 2022. Geochronology and geochemistry of the PiaOac granites: Implication for Late Cretaceous magmatism and metallogeny in NE Vietnam. Ore Geol. Rev. 142, 104727.

Peccerillo, A., Taylor, S.R., 1976. Geochemistry of Eocene calc-alkaline volcanic rocks from the Kastamonu area, Northern Turkey. Contrib. Miner. Petrol. 58, 63–81.

Qi, C.S., Deng, X.G., Li, W.X., Li, X.H., Yang, Y.H., Xie, L.W., 2007. Origin of the Darongshan-Shiwandashan S-type granitoid belt from southeastern Guangxi: geochemical and Sr-Nd-Hf isotopic constraints. Acta Petrol. Sin. 23, 403–412.

Richards, J.P., 2003. Tectono-magmatic precursors for porphyry Cu-(Mo-Au) deposit formation. Econ. Geol. 98, 1515–1533.

Richards, J.P., 2009. Postsubduction porphyry Cu–Au and epithermal Au deposits: Products of remelting of subduction–modified lithosphere. Geology 37, 247–250.

Richards, J.P., 2011. Magmatic to hydrothermal metal fluxes in convergent and collided margins. Ore Geol. Rev. 40, 1–26.

Richards, J.P., 2015. The oxidation state, and sulfur and Cu contents of arc magmas: implications for metallogeny. Lithos 233, 27-45.Richards, J.P., 2015b. Tectonic, magmatic, and metallogenic evolution of the Tethyan orogen: From subduction to collision. Ore Geology Reviews 70, 323-345. Richards, J.P., 2022. Porphyry copper deposit formation in arcs: What are the odds? Geosphere 18, 130–155.

Roger, F., Jolivet, M., Maluski, H., Respaut, P.J., Münch, P., Paquette, J.L., Tich, V.V., Vuong, N.V., 2014. Emplacement and cooling of the Dien Bien Phu granitic complex: Implications for the tectonic evolution of the Dien Bien Phu Fault (Truong Son Belt, NW Vietnam). Gondw. Res. 26, 785–801.

Romer, R.L., Hahne, K., 2010. Life of the Rheic Ocean: Scrolling through the shale record. Gondw. Res. 17, 236–253.

Romer, R.L., Kroner, U., 2016. Phanerozoic tin and tungsten mineralization—Tectonic controls on the distribution of enriched protoliths and heat sources for crustal melting. Gondw. Res. 31, 60–95.

Romer, R.L., Kroner, U., 2022. Provenance control on the distribution of endogenic Sn-W, Au, and U mineralization within the Gondwana-Laurussia plate boundary zone. In: Kuiper, Y.D., Murphy, J.B., Nance, R.D., Strachan, R.A., Thompson, M.D. (Eds.), New Developments in the Appalachian-Caledonian-Variscan Orogen: Geological Society of America Special Paper 554, pp. 25–46.

Rudnick, R., Gao, S., 2003. Composition of the continental crust. In: Rudnick, R.L. (Ed.), The Crust. Treatise on Geochemistry. Elsevier-Pergamon, Oxford, pp. 1–64 (Chap. 63).

Sato, K., 2012. Sedimentary Crust and Metallogeny of Granitoid Affinity: Implications from the Geotectonic Histories of the Circum-Japan Sea Region, Central Andes and Southeastern Australia. Resour. Geol. 62, 329–351.

Seedorff, E., Dilles, J.H., Proffett, J.M., Einaudi, M.T., Zurcher, L., Stavast, W.J.A., Johnson, D.A., Barton, M.D., 2005. Porphyry deposits: Characteristics and origin of hypogene features. Econ. Geol. 251–298.

Shi, Z.X., Gao, R., Lu, Z.W., Li, W.H., Li, H.Q., Huang, X.F., Liang, H.D., 2022. Bidirectional subduction of the Bangong–Nujiang ocean revealed by deep–crustal seismic reflection profile. Tectonophysics 837, 229455.

Shu, Q.H., Deng, J., Chang, Z.S., Wang, Q.F., Niu, X.D., Xing, K., Sun, X., Zhang, Z.K., Zeng, Q.W., Zhao, H.S., Yu, F., 2024. Skarn Zonation of the Giant Jiama Cu-Mo-Au Deposit in Southern Tibet, SW China. Econ. Geol. 119, 1–22.

Sinclair, W.D., 2007. Porphyry deposits. Mineral deposits of Canada: A synthesis of major deposit–types, district metallogeny, the evolution of geological provinces, and exploration methods. Geol Assoc Can, Min Dep Div, Spec Publ 5, 223–243.

Song, S.W., Mao, J.W., Yuan, S.D., Jian, W., 2022. Decoupling of Sn and W mineralization in a highly fractionated reduced granitic magma province: a case study from the Youjiang basin and Jiangnan tungsten belt. Miner. Deposita 57, 1251–1267.

Sun, X., Zheng, Y., Xu, J., Huang, L., Guo, F., Gao, S., 2017. Metallogenesis and ore controls of Cenozoic porphyry Mo deposits in the Gangdese belt of southern Tibet. Ore Geol. Rev. 81, 996–1014.

Sun, X., Hollings, P., Lu, Y.-J., 2021. Geology and origin of the Zhunuo porphyry copper deposit, Gangdese belt, southern Tibet. Miner. Deposita 56, 457–480.

Sun, X., Deng, J., Lu, Y., Si, X., Hollings, P., Santosh, M., Li, Q., Zheng, X., 2023. Two stages of porphyry Cu mineralization at Jiru in the Tibetan collisional orogen: Insights from zircon, apatite, and magmatic sulfides. GSA Bull.

Tang, J.X., Lang, X.H., Xie, F.W., Gao, Y.M., Li, Z.J., Huang, Y., Ding, F., Yang, H.H., Zhang, L., Wang, Q., Zhou, Y., 2015. Geological characteristics and genesis of the Jurassic No. I porphyry Cu–Au deposit in the Xiongcun district, Gangdese porphyry copper belt, Tibet. Ore Geology Reviews 70, 438–456.

Tang, J.X., Yang, H.H., Song, Y., Wang, L.Q., Liu, Z.B., Li, B.L., Lin, B., Peng, B., Wang, G. H., Zeng, Q.G., Wang, Q., Chen, W., Wang, N., Li, Z.J., Li, Y.B., Li, Y.B., Li, H.F., Lei, C.Y., 2021. The copper polymetallic deposits and resource potential in the Tibet Plateau. China Geology 4, 1–16.

Tian, H.-C., Tian, S.-H., Hou, Z.-Q., Yang, Z.-M., Zheng, Y., 2022. Lithium isotope fractionation during magmatic differentiation and hydrothermal processes in post-collisional adakitic rocks. Geochim. Cosmochim. Acta 332, 19–32.

Wai-Pan Ng, S., Chung, S.L., Robb, L.J., Searle, M.P., Ghani, A.A., Whitehouse, M.J., Oliver, G.J.H., Sone, M., Gardiner, N.J., Roselee, M.H., 2015. Petrogenesis of Malaysian granitoids in the Southeast Asian tin belt: Part 1. Geochemical and Sr-Nd isotopic characteristics. Geo. Soc. America Bullet. 127, 1209–1237.

Wang, X.-S., Hu, R.-Z., Bi, X.-W., Leng, C.-B., Pan, L.-C., Zhu, J.-J., Chen, Y.-W., 2014a. Petrogenesis of Late Cretaceous I-type granites in the southern Yidun Terrane: New constraints on the Late Mesozoic tectonic evolution of the eastern Tibetan Plateau. Lithos 208–209, 202–219.

Wang, D.-Z., Hu, R., Hollings, P., Bi, X.-W., Zhong, H., Pan, L.-C., Leng, C.-B., Huang, M.-L., Zhu, J.-J., 2021b. Remelting of a Neoproterozoic arc root: origin of the Pulang and Songnuo porphyry Cu deposits, Southwest China. Miner. Deposita 56, 1043–1070.

Wang, X.H., Lang, X.H., Turlin, F., Deng, Y.L., Xie, F.W., He, Q., Moritz, R., 2024. Copper behavior in arc-back-arc systems: Insights into the porphyry Cu metallogeny of the Gangdese belt, southern Tibet. Miner. Deposita 59, 133–154.

Wang, T.Y., Li, G.J., Wang, Q.F., Santosh, M., Zhang, Q.Z., Deng, J., 2019a. Petrogenesis and metallogenic implications of Late Cretaceous I- and S-type granites in Dachang–Kunlunguan ore belt, southwestern South China Block. Ore Geol. Rev. 113, 103079.

Wang, R., Richards, J.P., Hou, Z.Q., Yang, Z.M., Gou, Z.B., DuFrane, S.A., 2014b. Increasing magmatic oxidation state from Paleocene to Miocene in the eastern Gangdese belt, Tibet: implication for collision-related porphyry Cu-Mo Au mineralization. Econ. Geol. 109, 1943–1965.

Wang, R., Weinberg, R.F., Collins, W.J., Richards, J.P., Zhu, D.-C., 2018. Origin of postcollisional magmas and formation of porphyry Cu deposits in southern Tibet. Earth Sci. Rev. 181, 122–143.

Wang, R., Luo, C.-H., Xia, W.-J., He, W.-Y., Liu, B., Huang, M.-L., Hou, Z.-Q., Zhu, D.-C., 2021a. Role of Alkaline Magmatism in Formation of Porphyry Deposits in Nonarc Settings: Gangdese and Sanjiang Metallogenic Belts. Society of Economic Geologists, Special Publication, pp. 205–229.

Wang, X.S., Williams-Jones, A.E., Bi, X.W., Hu, R.Z., Xiao, J.F., Huang, M.L., 2019b. Late Cretaceous Transtension in the Eastern Tibetan Plateau: Evidence From Postcollisional A-Type Granite and Syenite in the Changdu Area, China. J. Geophys. Res. Solid Earth 124, 6409–6427.

Wang, Q.F., Yang, L., Xu, X.J., Santosh, M., Wang, Y.N., Wang, T.Y., Chen, F.G., Wang, R. X., Gao, L., Liu, X.F., Yang, S.J., Zeng, Y.S., Chen, J.H., Zhang, Q.Z., Deng, J., 2020a. Multi-stage tectonics and metallogeny associated with Phanerozoic evolution of the South China Block: A holistic perspective from the Youjiang Basin. Earth Sci. Rev. 211, 103405.

Wang, R., Zhang, J., 2025. Advances in origin of high oxidation state of magmas associated with porphyry Cu-(Mo-Au) deposits. Sci. China Earth Sci. 68, 953–956.

Wang, R., Zhu, D., Wang, Q., Hou, Z., Yang, Z., Zhao, Z., Mo, X., 2020b. Porphyry mineralization in the Tethyan orogen. Sci. China Earth Sci. 63, 2042–2067.

Whalen, J.B., Anderson, R.G., Struik, L.C., Villeneuve, M.E., 2001. Geochemistry and Nd isotopes of the François Lake plutonic suite, Endako batholith: host and progenitor to the Endako molybdenum camp, central British Columbia. Can. J. Earth Sci. 38, 603–618.

Wolf, M., Romer, R.L., Franz, L., López-Moro, F.J., 2018. Tin in granitic melts: The role of melting temperature and protolith composition. Lithos 310, 20–30.

Xu, J.F., Castillo, P.R., 2004. Geochemical and Nd–Pb isotopic characteristics of the Tethyan asthenosphere: implications for the origin of the Indian Ocean mantle domain. Tectonophysics 393, 9–27.

Xu, B., Hou, Z.-Q., Zheng, Y.-C., Wang, R., He, M.-Y., Zhou, L.-M., Wang, Z.-X., He, W.-Y., Zhou, Y., Yang, Y., 2017. In situ elemental and isotopic study of diorite intrusions: Implication for Jurassic arc magmatism and porphyry Cu-Au mineralisation in southern Tibet. Ore Geol. Rev. 90, 1063–1077.

Xu, M.J., Li, C., Zhang, X.Z., Wu, Y.W., 2014. Nature and evolution of the Neo-Tethys in central Tibet: synthesis of ophiolitic petrology, geochemistry, and geochronology. Int. Geol. Rev. 56, 1072–1096.

Xu, R., Romer, R.L., Kroner, U., Deng, J., 2022. Tectonic control on the spatial distribution of Sn mineralization in the Gejiu Sn district, China. Ore Geol. Rev. 148, 105004.

Xu, J., Xia, X.P., Lai, C., Long, X., Huang, C., 2019. When Did the Paleotethys Ailaoshan Ocean Close: New Insights From Detrital Zircon U-Pb age and Hf Isotopes. Tectonics 38, 1798–1823.

Xu, W.C., Zhang, H.F., Luo, B.J., Guo, L., Yang, H., 2015. Adakite-like geochemical signature produced by amphibole-dominated fractionation of arc magmas: An example from the Late Cretaceous magmatism in Gangdese belt, south Tibet. Lithos 232, 197–210.
Xu, P.-Y., Zheng, Y.-C., Yang, Z.-S., Hou, Z.-Q., Shen, Y., Wang, Z.-X., Wu, C.-D., Zhou, L.-M., 2020. Metallogeny of the continental collision-related Jiagang W-Mo deposit, Tibet: Evidence from geochronology and petrogenesis. Ore Geol. Rev. 122, 103519.
Xu, L.-L., Zhu, J.-J., Huang, M.-L., Pan, L.-C., Hu, R.Z., Bi, X.-W., 2023. Genesis of hydrous-oxidized parental magmas for porphyry Cu (Mo, Au) deposits in a postcollisional setting: examples from the Sanjiang region, SW China. Miner. Deposita 58, 161–196.
Yan, Q., Jiang, X., Li, W., Li, C., Yang, F., 2024. Genesis of alkaline porphyries and associated Cu–Au–Pb–Ag polymetallic mineralization in an intracontinental transpression setting: Example from the Yao'an volcano-plutonic complex in western Yangtze Craton, SW China. Ore Geol. Rev. 165, 105922.
Yang, Z., Cao, K., 2024. Post-collisional porphyry copper deposits in Tibet: An overview. Earth Sci. Rev. 258, 104954.
Yang, Z.M., Cooke, D.R., 2019. Porphyry Cu Deposits in China. Soc. Economic Geol., Spec. Pub. 22, 133–187.
Yang, L.-Q., He, W.-Y., Gao, X., Xie, S.-X., Yang, Z., 2018. Mesozoic multiple magmatism and porphyry–skarn Cu–polymetallic systems of the Yidun Terrane, Eastern Tethys: Implications for subduction- and transtension-related metallogeny. Gondw. Res. 62, 144–162.
Yang, Z.M., Hou, Z.Q., White, N.C., Chang, Z.S., Li, Z.Q., Song, Y.C., 2009. Geology of the post-collisional porphyry copper–molybdenum deposit at Qulong, Tibet. Ore Geol. Rev. 36, 133–159.
Yang, F.C., Li, W.C., Jiang, X.J., Li, C., Wang, Z.Q., Sun, H.Y., Zhou, J.-X., 2020b. Late Cretaceous granitic intrusions and associated deposits in the Yidun Arc of the eastern Tibetan Plateau. J. Asian Earth Sci. 192, 104249.
Yang, F.C., Li, W.C., Zhu, X.P., Liu, J., Jiang, X.J., Yang, H.B., Li, Y., 2022. Origin of the Bada porphyry Cu–Au deposit, eastern Tibet: Geology and isotope geochemistry (C–O–S–Pb) constraints. Ore Geol. Rev. 146, 104935.
Yang, Z.-M., Lu, Y.-J., Hou, Z.-Q., Chang, Z.-S., 2015. High-Mg Diorite from Qulong in Southern Tibet: Implications for the Genesis of Adakite-like Intrusions and Associated Porphyry Cu Deposits in Collisional Orogens. J. Petrol. 56, 227–254.
Yang, F.C., Romer, R.L., Glodny, J., Li, W.C., 2023. Magma and fluid sources in an intracontinental porphyry system: A case study of the Relin Mo-W(-Cu) deposit, southern Yidun terrane. SW China. Ore Geology Reviews 163, 105761.
Yang, C., Tang, J.X., Beaudoin, G., Song, Y., Lin, B., Wang, Q., Fang, X., 2020c. Geology and geochronology of the Tiegelongnan porphyry-epithermal Cu (Au) deposit, Tibet, China: Formation, exhumation and preservation history. Ore Geol. Rev. 123, 103575.
Yang, L., Wang, Q., Groves, D.I., Lu, S., Li, H., Wang, P., Deng, J., 2021. Multiple orogenic gold mineralization events in a collisional orogen: Insights from an extruded terrane along the southeastern margin of the Tibetan Plateau. J. Struct. Geol. 147, 104333.
Yang, G.-S., Wen, H.-J., Ren, T., Xu, S.-H., Wang, C.-Y., 2020a. Geochronology, geochemistry and Hf isotopic composition of Late Cretaceous Laojunshan granites in the western Cathaysia block of South China and their metallogenic and tectonic implications. Ore Geol. Rev. 117, 103297.
Yin, A., Harrison, T.M., 2000. Geologic evolution of the Himalayan-Tibetan orogen. Annu. Rev. Earth Planet. Sci. 28, 211–280.
Zartman, R.E., Doe, B.R., 1981. Plumbotectonics—the model. Tectonophysics 75, 135–162.
Zhang, D., Audétat, A., 2017. Chemistry, Mineralogy and Crystallization Conditions of Porphyry Mo-forming Magmas at Urad–Henderson and Silver Creek, Colorado, USA. J. Petrol. 58, 277–296.
Zhang, J.B., Wang, R., Hong, J., 2022a. Amphibole fractionation and its potential redox effect on arc crust: Evidence from the Kohistan arc cumulates. Am. Mineral. 107, 1779–1788.
Zhang, Q.W., Wang, Q.F., Li, G.J., Sun, X., Shu, Q.H., Deng, J., 2022b. Crucial control on magmatic-hydrothermal Sn deposit in the Tengchong block, SW China: Evidence from magma differentiation and zircon geochemistry. Geosci. Front. 13, 101401.
Zhao, X.-Y., Deng, M.-G., Li, W.-C., Tang, Y.-W., Zhang, D.-C., Han, S.-K., Song, W.-B., Zhang, Q.-G., Xu, J.-W., 2024b. In situ U–Pb dating of garnet, vesuvianite, and scheelite from the Nanyangtian tungsten deposit reveals an Early Cretaceous W mineralization event in Southeast Yunnan, China. Gondw. Res. 133, 72–90.
Zhao, T.Y., Feng, Q.L., Metcalfe, I., Milan, L.A., Liu, G.C., Zhang, Z.B., 2017. Detrital zircon U–Pb–Hf isotopes and provenance of Late Neoproterozoic and Early Paleozoic sediments of the Simao and Baoshan blocks, SW China: Implications for Proto–Tethys and Paleo–Tethys evolution and Gondwana reconstruction. Gondwana Res. 51, 193–208.
Zhao, Z., Hou, L., Ding, J., Zhang, Q., Wu, S., 2018. A genetic link between Late Cretaceous granitic magmatism and Sn mineralization in the southwestern South China Block: A case study of the Dulong Sn-dominant polymetallic deposit. Ore Geol. Rev. 93, 268–289.
Zhao, F., Yang, F., Xue, S., Wu, H., Li, W., Li, C., Yan, Q., Sun, Z., Tang, J., Jiang, L., 2024a. Magmatic evolution and metallogenic diversity of the late Cretaceous granites in the Yidun terrane: Constraints from zircon and apatite geochemistry. Ore Geol. Rev. 169, 106084.
Zhen, S.-M., Jia, W.-B., Wang, Z.-G., Han, Z.-H., Song, X.-H., Zhao, S.-C., 2021. The Oligocene tin mineralization in the SE Sanjiang metallogenic belt, SW China. China Geology 4, 1–3.
Zhu, J.-J., Hu, R., Richards, J.P., Bi, X., Zhong, H., 2015. Genesis and magmatic-hydrothermal evolution of the Yangla skarn Cu deposit, Southwest China. Econ. Geol. 110, 631–652.
Zhu, D.-C., Li, S.-M., Cawood, P.A., Wang, Q., Zhao, Z.-D., Liu, S.-A., Wang, L.-Q., 2016. Assembly of the Lhasa and Qiangtang terranes in central Tibet by divergent double subduction. Lithos 245, 7–17.
Zhu, Y.T., Li, X.F., Li, Z.F., 2022. The fractures-controlled tin mineralization at the end of Late Cretaceous in the Songshan deposit, southwestern China: Constraints from U–Pb dating of zircon, garnet, and cassiterite. Ore Geol. Rev. 150, 105191.
Zhu, Y.-S., Yang, J.-H., Sun, J.-F., Wang, H., 2017. Zircon Hf-O isotope evidence for recycled oceanic and continental crust in the sources of alkaline rocks. Geology 45, 407–410.
Zhu, D.-C., Zhao, Z.-D., Niu, Y., Mo, X.-X., Chung, S.-L., Hou, Z.-Q., Wang, L.-Q., Wu, F.-Y., 2011. The Lhasa Terrane: Record of a microcontinent and its histories of drift and growth. Earth Planet. Sci. Lett. 301, 241–255.